KOMEX

KURILE OKHOTSK SEA MARINE EXPERIMENT

CRUISE REPORTS: KOMEX I and II

RV PROFESSOR GAGARINSKY CRUISE 22
RV AKADEMIK M. A. LAVRENTYEV CRUISE 28

VLADIVOSTOK - PUSAN - OKHOTSK SEA - PUSAN - VLADIVOSTOK
7 JULY - 12 SEPTEMBER 1998

Edited by Nicole Biebow and Edna Hütten

The KOMEX I and II marine expeditions were initialized on responsibility of
the P. P. Shirshov Institute of Oceanology, Moscow,
the Pacific Oceanological Institute (POI), Vladivostok,
and the GEOMAR Research Center for Marine Geosciences, Kiel

GEOMAR
Forschungszentrum
für marine Geowissenschaften
der Christian-Albrechts-Universität
zu Kiel

KIEL 1999

GEOMAR REPORT 82

GEOMAR
Research Center
for Marine Geosciences
Christian Albrechts University
in Kiel

Redaktion dieses Reports:
Nicole Biebow und Edna Hütten

Editors of this issue:
Nicole Biebow and Edna Hütten

GEOMAR REPORT
ISSN 0936 - 5788

GEOMAR REPORT
ISSN 0936 - 5788

GEOMAR
Forschungszentrum
für marine Geowissenschaften
Wischhofstr. 1-3
D - 24148 Kiel
Tel. (0431) 600-2555, 600-2505

GEOMAR
Research Center
for Marine Geosciences
Wischhofstr. 1-3
D - 24148 Kiel
Tel. (49) 431 / 600-2555, 600-2505

Table of contents

APPENDICES

Preface: KOMEX: *K*urile *O*khotsk Sea *M*arine *EX*periment

N. Biebow and E. Suess

Bound by the Asian continent to the northwest and north and the Kurile-Kamchatka-Island Arc to the east and southeast, the Sea of Okhotsk is the second largest marginal sea of the Pacific Ocean. It is characterized by its complicated tectonic structure, its high methane production rate and seeping activity, its distinct seasonal character of climate and oceanography and its high level of primary productivity. Therefore it represents a climate-forcing and ecologically highly sensitive system which offers a unique opportunity to carry out multi-disciplinary geoscientific research. The tectonics, environment, and ecology of the Sea of Okhotsk and the adjacent Kurile Island Arc are thus of high priority to understand the global climate change.

The joint German- Russian project KOMEX (***K***urile ***O***khotsk Sea ***M***arine ***EX***periment) funded for the initial phase by the German Federal Ministry of Education, Science and Technology (BMBF) and the Russian Ministry of Science and Technology, addresses the following distinct features of the Sea of Okhotsk through cooperation of various Russian-German working groups:

The Sea of Okhotsk is characterized by the highest potential marine methane production rate in the northern hemisphere; its seasonal ice-cover regulates the gas exchange with the atmosphere in an extraordinary way.

- The shelf areas around Sakhalin, Magadan west of Kamchatka, the Kurile Island Arc and the Kurile-Kamchatka subduction zone belong to an area with exceptionally active methane and fluid vents. Here depositionally bound, fermentatively formed and subduction-induced fluid vents generate enormous reservoirs of CH_4, CO_2 and other dissolved trace components. They are in direct contact with the bottom water and in shelf areas with the atmosphere. The influence of submarine fluid vents on ecology, sedimentology, water chemistry and atmospheric trace gases is still unknown and one of the central questions of the KOMEX project.
- The margins of the Sea of Okhotsk contain gas hydrates. Fluctuations of deep-sea temperatures and sea level have an impact on the stability of gas hydrates on the shelf and slope areas. Methane is released in great quantities, which as a greenhouse gas contributes to the atmospheric warming in an accelerating feedback.
- The Kurile Island Arc is a 1200 km long subduction system and one of the most active volcanic regions on Earth. As the eastern boundary of the Sea of Okhotsk, this subduction zone has not only a significant influence on its geodynamic evolution but it also plays an important role in mass transfer and material cycling in this area. Since the

discovery of fluid venting in accretionary wedges in subduction systems, the origin and evolution of fluids is of central interest. The question wether the fluids are recycled back to the ocean and/or influence the geochemical signature of the island arc magma is of major interest as well. For understanding and assessing the marine biogeochemical cycle it is of crucial importance to know and quantify not only the sedimentological but also the magmatic components. Additionally the input of volatiles and readily volatile elements into the atmosphere by volcanic eruptions is of importance and influences the global climate significantly. The Kurile Island Arc is an excellent area to study the influence of an active subduction system on the hydrosphere's and atmosphere's geochemical cycle, because it includes magmatic, hydrographic and atmospheric sources and sinks.

The Sea of Okhotsk covers an area equal the size of the North Sea and the Baltic Sea combined. To the east, the Sea of Okhotsk is bordered by the Kamchatka Penisula and the Kurile Island Arc. The water exchange through numerous straits into the open Pacific has a considerable impact on the circulation and intermediate-water formation in the western Pacific. Therefore, this exchange affects the oceanography and climate of the entire northwestern Pacific region. Additionally, the Sea of Okhotsk plays a crucial role as an interglacial high production zone which counteracts the natural atmospheric CO_2 increase during the late Quaternary melting periods and the succeeding interglacials. Several aspects of the influence of environmental parameters on the ocean-climate system in high latitudes can be studied in the Sea of Okhotsk:

- The Amur River is the only large Sibirian river which does not drain into the Arctic Ocean. Thus, a direct link between land covered with ice and the Pacific Ocean has existed during ice ages. This allows the reconstruction of terrestrial-marine interactions under glacial and interglacial conditions.

- From December to April each year the Sea of Okhotsk is largely ice-covered. During this period cold water flows into the Pacific Ocean. During glacial periods in contrast, the Sea of Okhotsk was completely ice-covered. Thus, the climatic change from glacial to interglacial periods has important effects on the production of cold water masses in the NW-Pacific which can be reconstructed from sediment records.

- The Sea of Okhotsk is characterized by an extremely high primary productivity, which has a seasonal character and is dominated by silicious plankton. Bathymetry and water depth of the Sea of Okhotsk are highly variable. Therefore, several types of sediment facies ranging from pelagic muds to organic-rich slope sediments are deposited. This variety of biogenic sediment facies presents an excellent opportunity to study paleoceanographical time slices with different resolutions. Meltwater influence, ice cover,

river input, and glacial-interglacial changes are controlling mechanisms for bioproduction, especially for the carbon and silica cycles.

The Kuriles form a characteristic island arc in the northwestern Pacific under which the oldest parts of the Pacific plate are subducted. Currently it is unclear, if the marginal sea was formed as a typical backarc basin with an opening at the northern border of the Kurile Basin or if it is an independent microplate.

- The plate tectonic character, the Sea of Okhotsk's age and the structure of the geologic margins and underlying basement are major topics of the geophysical and geological investigations as well as

- the investigation of the Kurile Island Arc magmatic rocks to characterize the plate-tectonic situation by their geochemical signature.

Those manifold objectives of the KOMEX project in this key area of the system earth can only be achieved by a multidisciplinary approach. Therefore, Russian-German working groups include geologists, geochemists, geophysicists, sedimentologists, paleontologists, paleoceanographers, volcanologists, biogeochemists and oceanographers. A successful base has been laid for the project in several pilot studies between 1992-1997. Interdisciplinary cooperation was established in July/August 1992 during the first joint expedition aboard *R V Akademik Nesmeyanov* which included scientists of the Pacific Oceanological Institute (POI, Vladivostok), the National Research Institute of Marine Fisheries and Oceanography (VNIRO, Moscow) and GEOMAR. This was followed by a short ice-expedition during the winter months to sample gases under the ice cover of the Sea of Okhotsk north of Sakhalin. The workshop on the Russian-German Cooperation in the Sea of Okhotsk-Kurile Island Arc was held in Moscow in November 1993 to compile the scientific results from the working area, especially from former studies of Russian partners and to define the common research topics and scientific objectives. Results of this workshop were integrated into the mature project.
In September/October 1994 the EC (INTAS)-funded expedition POSETIV (Paramushir-Okhotsk Sea Expedition to Investigate Venting) was carried out by the Pacific Oceanological Institute (Vladivostok), the Institute for Geophysics and Geology (Yuzhno-Sakhalinsk) and the P.P. Shirshov Institute (Moscow) with the participation of the Depts. of Marine Geology of the Netherlands Institute of Sea Research (NIOZ). In August 1995, another joint expedition, GERDA (Geophyical Researches in the Derugin Basin Area), took place. GEOMAR, the P.P. Shirshov Institute of Oceanology and the Pacific Oceanological Institute participated as well as Tokyo University. The program was mainly financed by GEOMAR and Tokyo University. Finally, in August/September 1996 another BMBF-financed expedition, GREGORY (German-Russian Expedition for Geological/Geophyical Okhotsk Sea Research) took place with the

participation of the Far Eastern Geological Institute and the Pacific Oceanological Institute (Vladivostok), the P.P. Shirshov Institute (Moscow) and GEOMAR. Important insights into the working area have been obtained thanks to these findings, data sets, and sample collections, and to the initiation of a Russian-German cooperation based on mutual trust and understanding. These conditions and experiences are the basis for a close cooperation which has been cultivated and will now be continued under the project KOMEX.

Due to distinct logistical demands of the different working groups, two expeditions with research vessels of the Pacific Oceanological Institute based in Vladivostok, will take place each year. The first cruise on board *RV Professor Gagarinsky* will focus on tectonic and structural objectives as well as on the detection and mapping of possible seafloor seepage areas. These investigations will provide the basic data for the second cruise aboard *RV Akademik Lavrentyev* with more marine-geological, geochemical and oceanographic objectives. During this cruise, seeping areas will be studied in detail by video-controlled systems. Besides water and plankton sampling as well as geological sampling for vent-geology, paleoceanology and volcanology programmes will be carried out.

Accordingly, the first joint KOMEX cruise in 1998 aboard *RV Professor Gagarinsky* took place from July 7th to August 10th 1998 followed by the second joint KOMEX cruise aboard *RV Akademik Lavrentyev* which departed from Vladivostok on August 7th and returned on September 12th 1998. The following report provides the results of these expeditions in two parts; including details of the participating institutions, the working groups and initial interpretations of the main findings.

PART I:

RV PROFESSOR GAGARINSKY CRUISE 22

CRUISE REPORT KOMEX I:

INESSA

INVESTIGATION OF EASTERN SAKHALIN SEEPAGE AREAS

VLADIVOSTOK - PUSAN - SEA OF OKHOTSK - PUSAN - VLADIVOSTOK

JULY 7 - AUGUST 10, 1998

1. Introduction and Background

B.V. Baranov, B.Ya. Karp, H.K. Wong, and S. Lammers

1.1 Tectonics

From the tectonic and geodynamic point of view, the Okhotsk Sea is a region of great interest. This sea occupies the bulk of the separate Okhotsk plate which is squeezed between four major plates: the North American, Eurasian, Pacific and Amurian plates (Fig. 1.1).

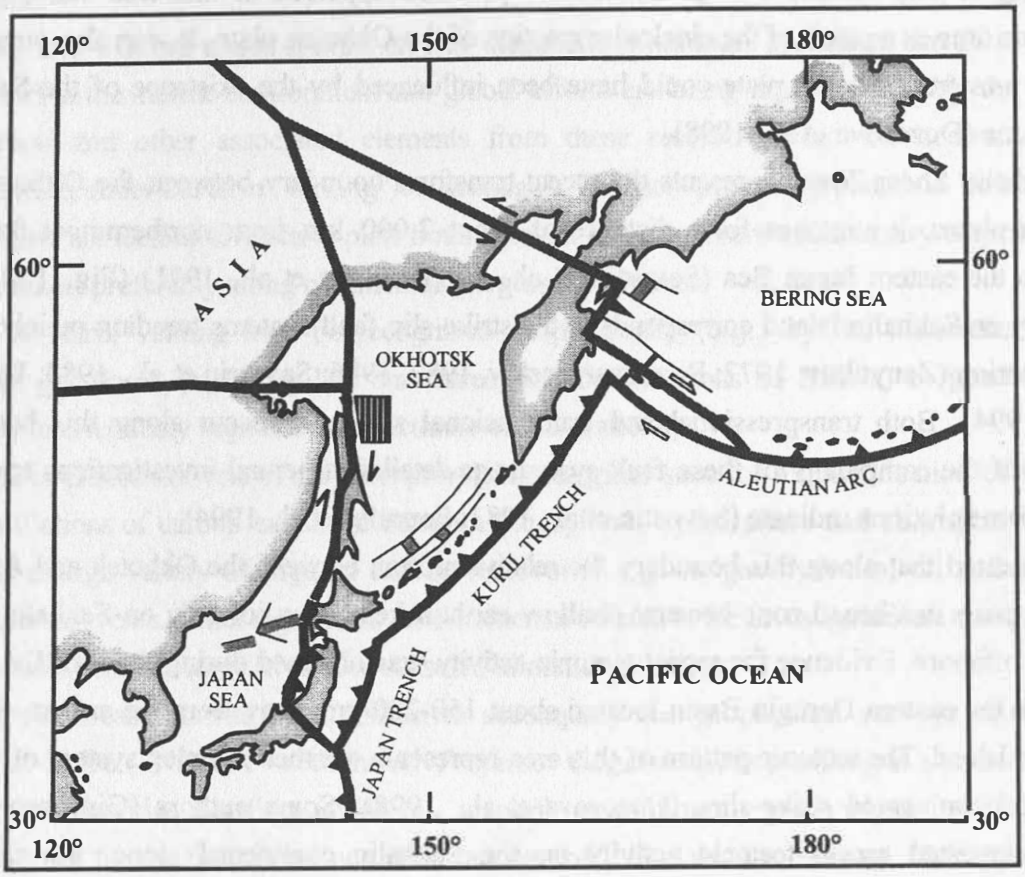

Fig. 1.1: Location of the INESSA study area (shaded) and recent plate geometry of the northwestern Pacific. The Okhotsk plate corresponds to the Okhotsk Sea and parts of the adjacent land areas. Dark gray lines with teeth indicate subduction zones with arrows marking the strike-slip boundaries. Light gray lines show inactive spreading axes in backarc areas (as suggested for the Okhotsk Sea). Thick black lines indicate recent extensional axes in the western Bering Sea.

Therefore, the geodynamics of the Okhotsk plate are closely connected with the character of relative movements between these plates and the Okhotsk Sea can be regarded as a key region for a better understanding of the geodynamics of northwestern Asia as a whole.

During the past three years, two cruises have been carried out in the Okhotsk Sea: Cruise 16 of the *RV Professor Gagarinsky* (1995) in the eastern Derugin Basin (Gerda Report, 1995) and Cruise 27 of the *RV Akademik M. A. Lavrentyev* (1996) in the central sea and on the

northwestern slope of the Kurile Basin (Nürnberg et al., 1996). These cruises were organized within the framework of the German-Russian scientific cooperation between GEOMAR (Kiel), POI (Vladivostok) and IORAS (Moscow) and represented the pilot and initial phase of the KOMEX project.

The data obtained in these two cruises provide evidence to support the Okhotsk Rift System and Kurile Basin opening model which have been developed recently (Baranov et al., 1995). According to this model, a large extensional province appeared in this area starting from Paleogene time as a result of the clockwise rotation of the Okhotsk plate. It was also suggested that the western Okhotsk plate could have been influenced by the existence of the Sakhalin Shear Zone (Dozorova et al., 1998).

The Sakhalin Shear Zone represents the recent transform boundary between the Okhotsk and Amurian plates. It stretches for a distance of about 2,000 km from northernmost Sakhalin Island to the eastern Japan Sea (Savostin et al., 1983; Jolivet et al., 1991) (Fig. 1.1). This boundary on Sakhalin Island corresponds to the strike-slip fault systems trending mainly in the N-S direction (Zanyukov, 1972; Rozhdestvenskiy, 1982, 1986; Savostin et al., 1983; Fournier et al., 1994). Both transpressional and transtensional structures occur along this boundary because of the complexity of these fault systems as detailed structural investigations and focal mechanism solutions indicate (Savostin et al., 1983; Fournier et al., 1994).

It is suggested that along this boundary the relative motion between the Okhotsk and Amurian plates appears in a broad zone because shallow earthquakes occur not only on Sakhalin Island but also offshore. Evidence for recent tectonic activity was obtained during the GERDA cruise (1995) in the eastern Derugin Basin located about 150-200 km away from the eastern coast of Sakhalin Island. The tectonic pattern of this area represents a rather complex system of normal faults and conjugated strike-slips (Dozorova et al., 1998). Some authors (Ginsburg et al., 1993) suggested recent tectonic activity on the Sakhalin continental slope, but the fault kinematics of this area are still uncertain.

Recent faults in the eastern offshore area of Sakhalin may serve as conduits for gas penetration to the sea floor. Two seepage areas located off northern Sakhalin were known and investigated before (Ginsburg et al., 1993) and a third one was found on the GREGORY cruise (1996) near southern Sakhalin (Nürnberg et al., 1996). It is well known that gas seeps are widespread on the inner slopes of trenches (subduction zones) and are connected with the existing fault pattern and the stress regime as was shown during submersible investigations of the Japan and Nankai Trenches (Kaiko-Tokai meeting, 1998). The offshore eastern Sakhalin region is related to another type of plate boundary, viz. a transform boundary, and detailed mapping of these seeps can be very useful in understanding the tectonic regime of this zone.

1.2 Methane and carbon dioxide in surface waters

An important objective of cruise 22 of the *RV Professor Gagarinsky* is the quantification of the sources and sinks of CH_4 and CO_2, geochemical end-members in both the production and decomposition of organic matter as well as the most important atmospheric trace gases. This task includes geochemical investigations of the cycling within the water column as well as the estimation of the transport rates between the sea and the atmosphere, which are primarily driven by the saturation gradients between the surface water and the atmospheric partial pressures of the gases.

As CH_4 and CO_2 are major components in diagenetic processes, sediments are their primary reservoirs in the marine environment and global efforts are being made to quantify the re-entry of carbon and other associated elements from these reservoirs into the oceans, usually summarized under the term "venting" or "seepage". The most promising places to investigate in this respect are tectonically active plate boundaries in regions where sedimentary organic matter accumulates, preferably along continental margins and shelves.

Areas of active venting may be recognized geophysically (e.g., by the occurrence of gas pockets, gas flares, pockmark-like structures, and deformations of BSR's) or geochemically (e.g., by anomalously high ambient methane concentrations).

The Sea of Okhotsk is one of the most promising marginal seas for a quantification of the rates and oscillations of carbon exchange between lithosphere, hydrosphere and atmosphere since it features a large variety of organic carbon reservoirs, e.g. as gas hydrates, oil and gas, and hydrothermal vents. Other significant environmental effects to be investigated are the supply of freshwater from the Amur River and seasonal climatic variations.

The air-sea measurements were chosen to accompany the geophysical surveys on the first KOMEX cruise - INESSA - with the *RV Professor Gagarinsky*, as profiling at a constant speed of 5 knots provides excellent conditions to perform continuous gas analyses of the surface waters. Also, for the first time since 1992, an area off NE Sakhalin between 52.5°-53.3°N and 143°-144.5°W could now be surveyed again. This area was previously found to be a net source of atmospheric methane (Lammers et al., 1995).

1.3 Objectives

The INESSA (INvestigation of the East Sakhalin Seepage Area) area of cruise 22 of the *RV Professor Gagarinsky* is located on the eastern slope off northern Sakhalin Island. The geophysical surveys in this cruise have the following main objectives:

- to elaborate on the tectonic pattern of the Sakhalin continental slope near seepage areas and to compare it with structures observed on Sakhalin Island itself;
- to obtain regional seismic cross-sections for seismic facies and sequence analyses and studies on sea level fluctuations;
- to investigate the known areas of gas seeps as well as to find new seepage areas; and

- to prepare recommendations for the forthcoming geological cruise on the *RV Akademik Lavrentyev* on the choice of the best sites for TV observations, coring and water sampling.

2. INSTRUMENTS AND METHODS

By B. Ya. Karp, S. Lammers, T. Lüdmann, H. K. Wong, A. Sudakov, and S. M. Nikolaev

2.1 Geophysical survey

A basic tool for the interpretation of seismic data is the concept of seismic stratigraphy. Reflections from the subsurface generated at sedimentary or structural interfaces with a significant change in acoustic impedance can be classified according to their external geometries, termination patterns (onlap, offlap etc.) and internal reflection configurations. Each succession of relatively conformable reflectors bounded at its top and base by unconformities or their correlative conformities is interpreted to correspond to a depositional sequence. Such a sequence is chronostratigraphically significant because it is deposited during a given interval of geologic time defined by ages of the sequence boundaries. Differences in internal reflection configuration, amplitude, continuity and frequency content between sequences suggest changes in the seismic facies, and these are attributed to changes in the depo-environment. Thus, seismo-stratigraphic interpretations provide an important tool for the reconstruction of the tectonic regime and the paleo-environment of an area.

The equipment used during the 1998 cruise of the *RV Professor Gagarinsky* includes

- a seismic reflection system consisting of a two-GI-gun array, an 8 channel mini-streamer, a multi-channel digital data acquisition system, an air gun trigger unit, a pressurized air distribution board and a linescan recorder. A single-channel digital data acquisition system permits real-time data monitoring (quality control) on screen and profile hard-copy printout on a line printer. Each of the S.S.I. GI-guns deployed has a maximum volume of 2.5 *l* (45 + 105 cu. in.). The two-gun array was pressurized nominally at 150 bar, towed behind the ship and triggered at 10.8 second intervals (every 25m at 4.5 knots) along prescribed profiles with pulses generated by a master clock. Each active channel of the GECO PRAKLA 8-channel mini-streamer has a length of 12.5 m.

  The operational characteristics of the multi-channel seismic reflection system are summarized in Tab. 2.1.

Table 2.1: Operational characteristics of the multi-channel seismic reflection system.

Source	
Type	2 × GI 45/105
Pressure	150 bar nominal
Firing interval	10.8 sec
Source depth	
Streamer	
First channel offset	150 m
No. of channels	8
Length of active section	12.5 m
Length of inactive section between active sections	12.5 m
Streamer depth	ca. 10 m
Recording	
Recording length	8 sec
Sampling frequency	1000 Hz
Bandpass analog filter	18-250 Hz

On the one hand, signals from the eight channels are separately digitized via a PC-based A/D converter board, multiplexed, and written onto high capacity EXABYTE tapes. Back in the home laboratory, the data will be demultiplexed and transformed to the standard SEGY format. They will then be processed using the *iXL* seismic processing software package. The processing steps include sorting, digital filtering, NMO-correction, stacking, deconvolution and migration. On the other hand, the incoming analog signals from the different channels of the streamer are summed, amplified, bandpass filtered (15-350 Hz), and written onto a DAT-tape for archiving, displayed online on an EPC 4800 graphic recorder, as well as directed to the single-channel digital data acquisition system for monitoring and data storage.

- a single channel seismic reflection system made up of a 3 *l* air gun, a streamer, an amplifier-filter system, and a single-channel digital data acquisition system based on a commercial sound card (Sound Blaster Pro) which writes the analog signal on the harddisk of a 386-PC (see Tab. 2.1 for characteristics). Simultaneously, 620 traces were displayed on the computer monitor. Backups were made offline on magneto-optical disks. On/off switching of the seismic recording on harddisk, on-screen seismic signal display and the adjustment of the dynamic range of the seismic signal were controlled by software developed for this purpose.

Table 2: Specification of the single-channel data acquisition system.

Length of trace	4 sec.
Start delay	optional from 0 to 2 sec in 1 sec steps
Sampling rate	optional from 0.05 ms to 2 ms; here: 2 ms
Data format	8 bits sign

- a 2-12 kHz echosounder system consisting of a towed, four element transducer, a transmitter with a power output of 10 kW at 0.75 % duty cycle, a receiver, a digital data acquisition system and a linescan recorder. The output frequency of the system is adjustable between 2-12 kHz, and the pulse width may be varied within the range of 1-32 cycles of the frequency selected. In addition, the functions of gain, time-varied gain with adjustable delay, AGC, bandpass filtering, key programming and swell compensation are integrated;
- an analog sidescan sonar system for shallow water applications which consists of a towed transducer with depressor, a transceiver, a 4-channel DAT-recorder and an analog monitoring system. The towed, variable beam transducers have a horizontal beam width of 1° and a pulse width of 0.1 ms at an output frequency of 100 kHz. The beams can be tilted down either 0°, 10° or 20° below the horizontal and the vertical beam width is adjustable to a value of 20° or 40°;
- a Russian, surface-towed, MBM-1™ marine proton magnetometer for magnetic total intensity measurements. This magnetometer has a measuring range of 20,000-100,000 nT and an accuracy of 2-4 nT over its entire measuring range. The magnetometer sensor was towed by a non-magnetic cable at a distance of 250 m behind the ship. The magnetic data were written on an analogue recorder for visual display and stored on an IBM PC-386 at a sampling rate of 10 seconds;
- a Russian shipboard gravity meter consisting of four highly-damped, spring-type GMN™ marine gravimeters mounted on GMS-2™ gyrostabilized platforms installed in a special laboratory on board. The gravimeters achieved an accuracy of 0.8 mgal. In order to reduce cross-coupling errors, a straight-line model of two gravimeters was used. The gravity data were written on an analogue recorder for visual inspection and stored on an IBM PC-386 at a sampling rate of 4 seconds. Gravity observations were started at the pier in Vladivostok at a gravity base station three days before the beginning of the cruise;
- a Russian GEL-3™ wide-beam echo-sounder for bathymetric measurements. This echo-sounder has a measuring range of up to 10 km water depth and operates at a frequency of 12.4 kHz. The water depths were recorded on an analogue echograph which was then sampled manually every 5 minutes; and

- a shipboard global positioning system.

2.2 Gas survey

Saturations of dissolved methane and carbon dioxide in the surface waters were measured using a flow-through system that maintains equilibrium between continuously pumped surface seawater and air. CH_4 and CO_2 concentrations could be sequentially measured in an equilibrated gas phase as well as in air and, by taking temperature differences into account, the saturation of both species relative to their partial pressures in the ambient atmosphere could be calculated (for further details of the system see Rehder, 1996).

Sequences of air, equilibrated air, and two different gas standards were sequentially introduced into a two-channel gas-chromatograph (SRI 8610C) and detected by flame- ionisation-detection (FID). A catalytic reduction to CH_4 (by means of a H_2-fed Ni-catalyst at 380° C) made the CO_2 detectable by flame-ionisation. From the multiple gas analyses, standard deviations were found to be less than 1.2% for methane and less than 0.6% for carbon dioxide.
The system was adjusted to record the water values at intervals of 8 minutes, i.e., with a resolution of 0.67 nm at an average speed of 5 knots. The GC analyses were accompanied by sensor recordings of the salinity, temperature, and pH of the supplied seawater. Both data acquisition and system control were performed by the SRI-PeakSimple software installed on a laptop computer.

3. RESULTS

3.1 Seismic stratigraphy of the different physiographic provinces

By B. Ya. Karp, H. K. Wong, T. Lüdmann, and V. N. Karnaukh

3.1.1 Basinal province

The sedimentary column of the basinal province of the Derugin Basin ranges in thickness from 0.6 to >2.3 s TWT depending on the topography of the acoustic basement. This basement is characterized either by finely stratified reflectors, or an envelope of diffraction hyperbolas, or opaque reflectors (lacking any further penetration). Asymmetric blocks and relatively symmetric highs can be recognized.

The basinal province of the Derugin Basin studied can be divided into three areas, each having its own distinct seismo-stratigraphic characteristics (Fig. 3.1). The first (area I) lies in the south. Its sedimentary section comprises four seismic units: two well-stratified sequences and two semi-transparent sequences (profile 3, Figs. 3.2 and 3.3). The upper well-stratified sequence consists of subparallel seismic reflections. The total sequence thickness is 0.3-0.6 s, increasing progressively to the south. A flat-lying high amplitude reflector running subparallel to the seafloor occurs near its lower boundary (BSR). The upper semi-transparent sequence has only occasional, low amplitude, discontinuous reflectors. The sequence thickness is 0.24-0.35 s. A second BSR is found within this sequence. The lower well-stratified sequence is distinguishable from its upper counterpart in that subparallel reflections are grouped into several subsequences separated by transparent layers. In all, four subsequences bounded by minor unconformities are present. In places, the reflection pattern of this sequence suggests regional subsidence. The sequence thickness varies from 0.6 to 1.4 s. The lower semi-transparent sequence, with a thickness of 0.2-0.3 s TWT, exhibits the same seismic facies characteristics as its upper counterpart. Numerous small erosional channels dissect the seafloor in the southern part of this area (profile 3, Fig. 3.3) according to our new (this cruise) and old (GERDA expedition) seismic data.

The sedimentary section of area II is characterized by the presence of a medium amplitude, acoustically turbid sequence (B2) lacking any significant internal structures and bounded above by a distinct erosional truncation (profile 40, Fig. 3.4). This sequence is overlain by a thin, well-stratified, onlapping sediment fill of the youngest sequence B1. Underlying the turbid facies B2 is likewise a well-stratified sequence B3. Its upper part is laterally discontinuous and occurs as a basinal fill, while its lower part is represented by well-stratified, high amplitude reflectors exhibiting antiforms that are progressively more distinct with depth. The next stratigraphically older sequence (B4) is semi-transparent with only occasional, more-or-less conformal internal reflections reminiscent of hemi-pelagic sedimentation. It is underlain by sequence B5, the facies of which is very similar to that of the lower section of B3. The oldest

sequence penetrated (B6) is characterized by strong, intermittent reflectors that are often hyperbolic.

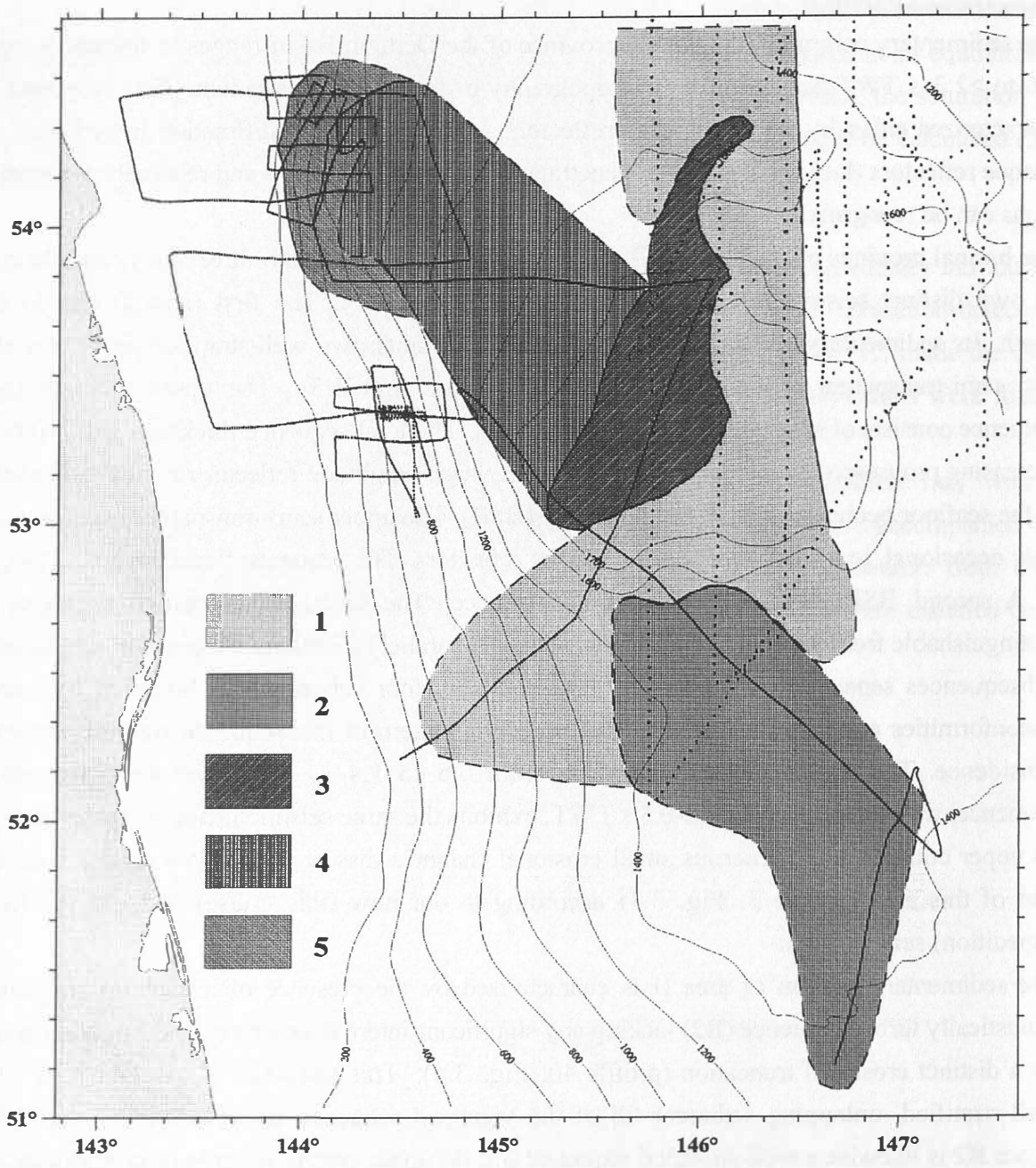

Fig. 3.1: Map of the location of areas with different seismo-stratigraphic characteristics. 1=area I; 2=area I with erosional channels incised into the seafloor; 3=area II; 4=area III; 5=young, lenticular sedimentary body; see text for explanation. Thick continuous lines give the location of profiles, present study (INESSA cruise); dotted lines that of the GERDA cruise. Thin continuous lines are isobaths in meters.

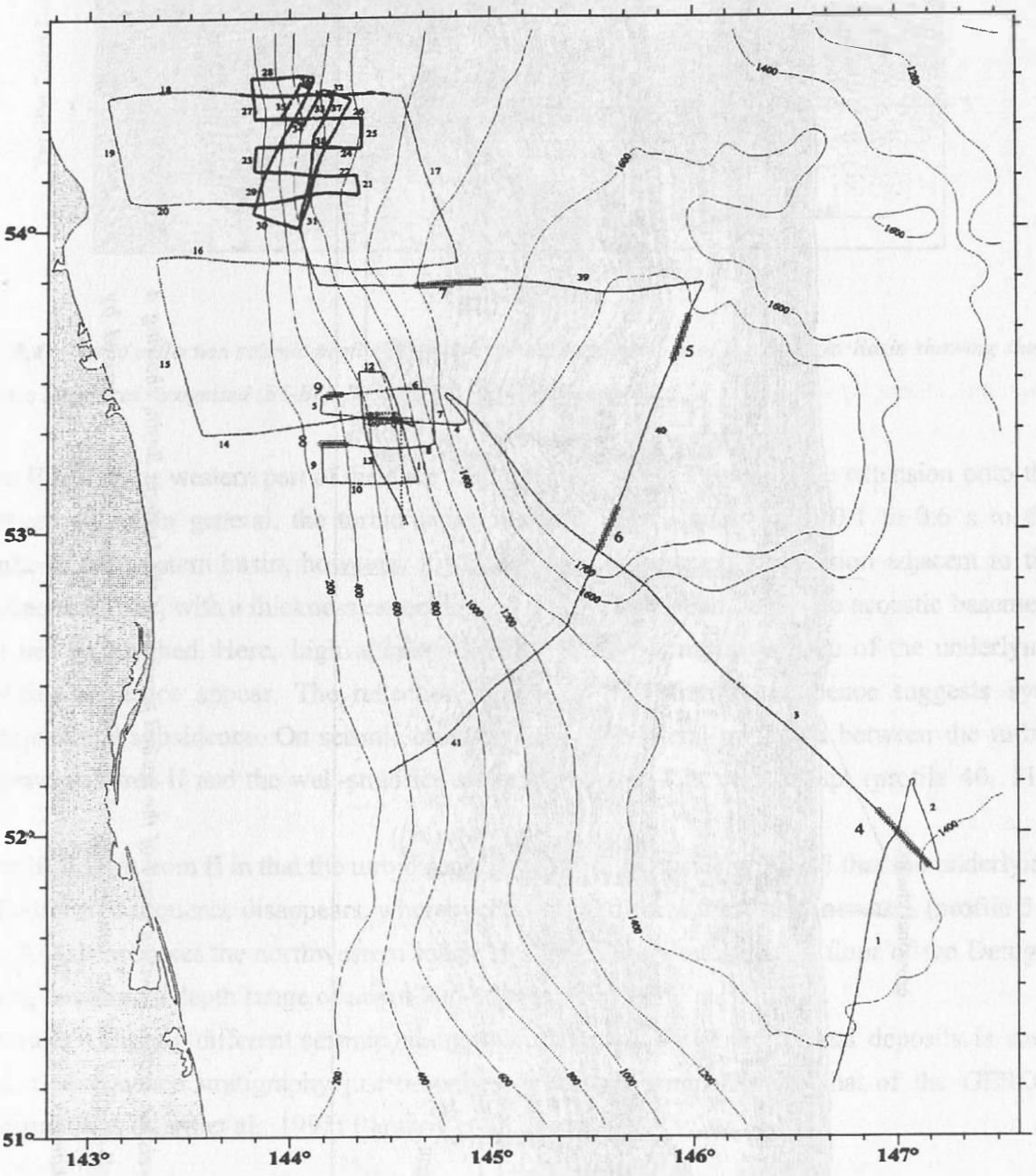

Fig. 3.2: Location of the selected profiles shown in Figs. 3.3-3.8 (large numbers). Small numbers are profile numbers.

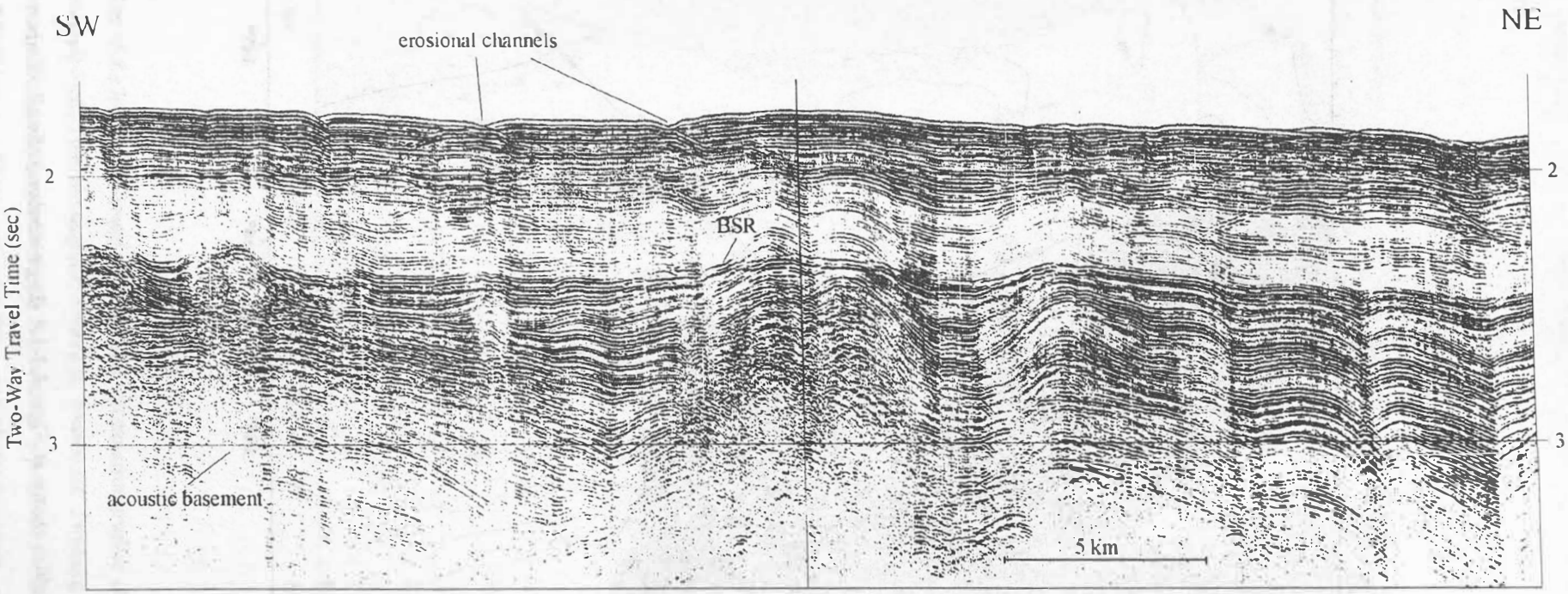

Fig. 3.3: *Reflection seismic profile 3 within area I of the basinal province of the Derugin Basin, showing a succession of two well-stratified and two semi-transparent sequences. Note that the seafloor is incised by numerous erosional channels. See Fig. 3.2 for profile location.*

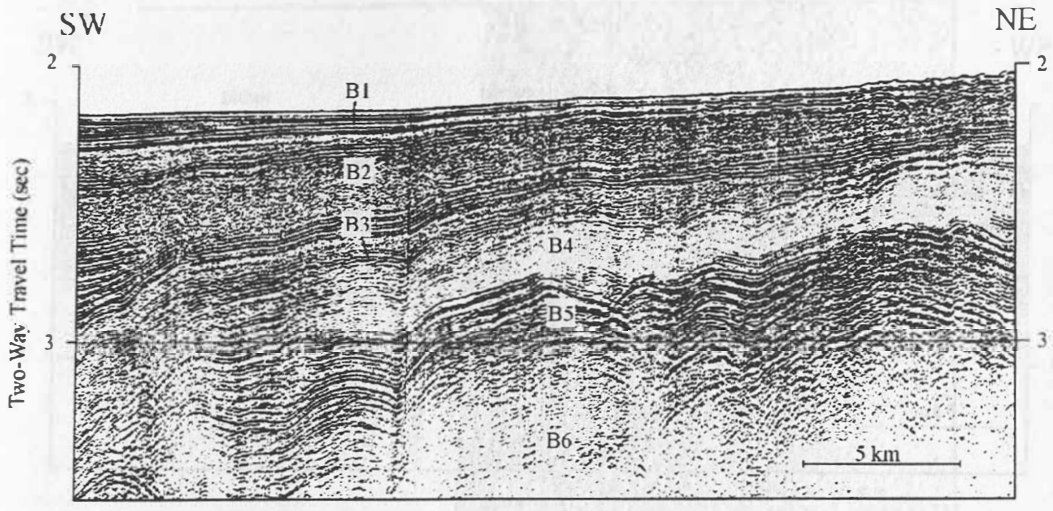

Fig. 3.4: *Part of reflection seismic profile 40 within the basinal province of the Derugin Basin showing the 6 seismic sequences recognized (B1-B6). See Fig. 3.2 for profile location.*

Area II lies in the western part of the deep Derugin Basin with a tongue-like extension onto the northern slope. In general, the turbid facies increases in thickness from 0.1 to 0.6 s to the south. In the western basin, however, it fills an acoustic basement depression adjacent to the continental slope, with a thickness exceeding 2.1 s TWT, at which depth the acoustic basement was not yet reached. Here, high amplitude reflectors conformal to the top of the underlying stratified sequence appear. The reflection pattern of this stratified sequence suggests syn-deformational subsidence. On seismic cross-sections, the lateral transition between the turbid sequence of area II and the well-stratified sequence of area I is very abrupt (profile 40, Fig. 3.5).

Area III differs from II in that the turbid sequence thickens considerably and that the underlying well-stratified sequence disappears, whereby the total sediment thickness increases (profile 39, Fig. 3.6). It occupies the northwestern lower slope and the western basin floor of the Derugin Basin, covering a depth range of about 700-1700 m (Fig. 3.1).

Although a slightly different seismic stratigraphic subdivision of the basinal deposits is used here, the sequence stratigraphy just described is directly comparable to that of the GERDA investigations (Karp et al., 1995; Baranov et al., in press).

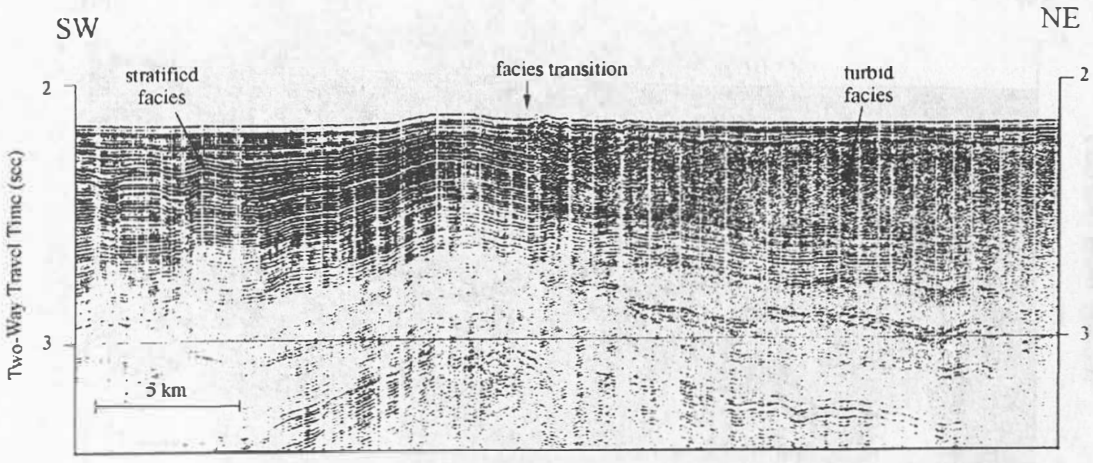

Fig. 3.5: *Part of reflection seismic profile 40 on the southwestern slope of the Derugin Basin showing the transition between the turbid facies and the well-straified facies. See Fig. 3.2 for profile location.*

3.1.2 Western slope of the Derugin Basin

The well-stratified sedimentary unit SL to which the turbid facies also grades in the southern seepage area consists of a series of parallel reflectors of differing amplitudes and frequency contents. It is, however, very difficult to subdivide into sequences despite its thickness of >1 sec TWT. This is because unconformities which function as sequence boundaries are here difficult to recognize (profile 8, Fig. 3.7).

Firstly, the occurrence of gas in the sediments results in phenomena such as acoustic masking and velocity pull-down (or pull-up) with apparent bending and interruption of the stratal interfaces. Secondly, the BSR's are subparallel to the seafloor and therefore intersect the strata only at an oblique angle, making true, low angle unconformities difficult to discern. Lastly, landwards at about 350 m water depth, the seafloor descends in a series of steps (e.g., profile 8) each of which marks an en echelon normal fault with a small throw (3.5 kHz echosounder profile 6, Fig. 3.8). These normal faults produce reflections and diffractions that are oblique and dissect the prominent stratal horizons into short, offset segments. Again, unconformities would be hard to recognize under these conditions.

At the northern seepage area, the youngest sequence constitutes a lenticular sedimentary body that occupies that upper basinal slope (Fig. 3.1). This lens does not continue into the southern seepage area.

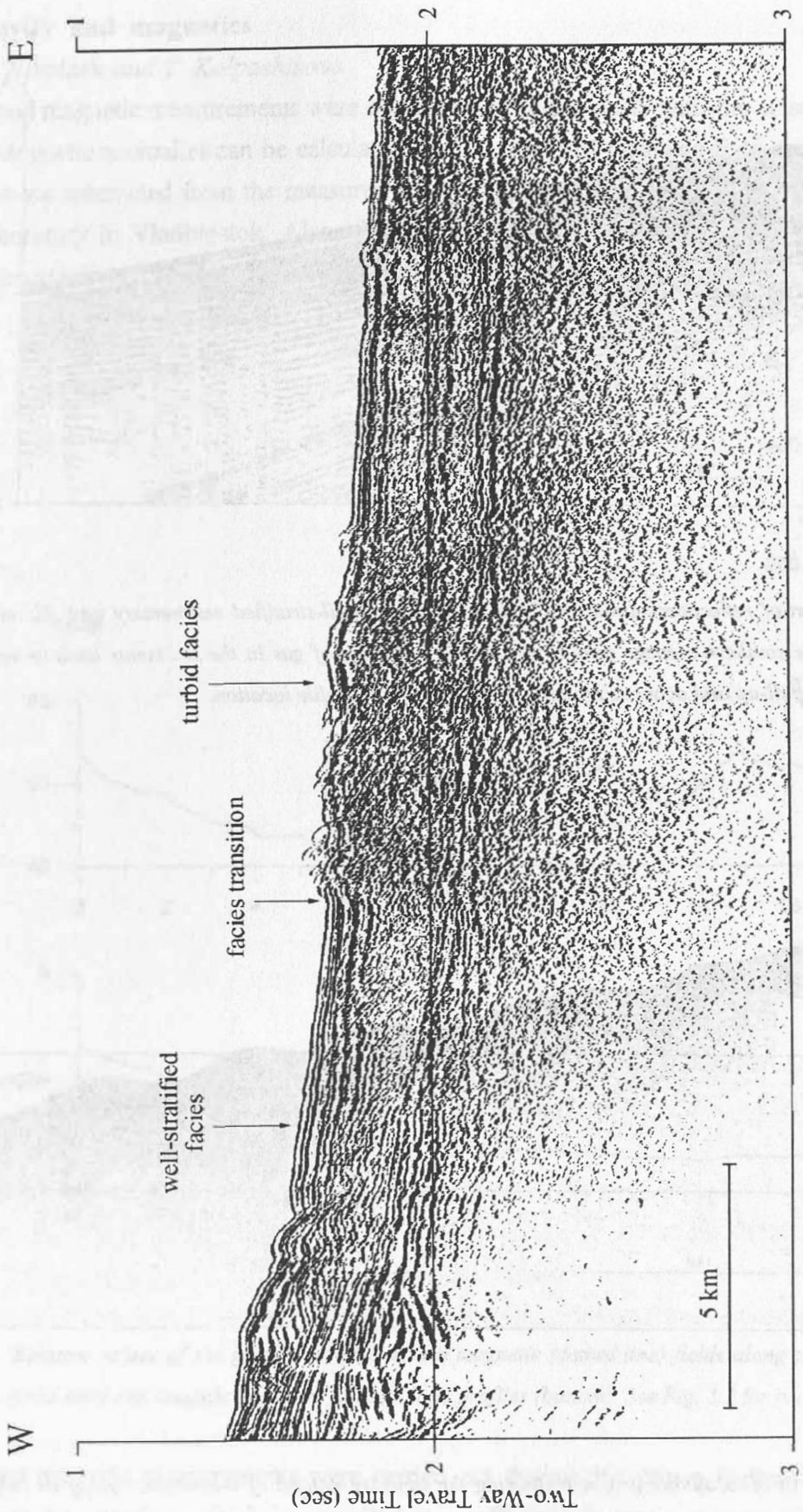

Fig. 3.6: Part of reflection seismic profile 39 on the southwestern slope of the Derugin Basin showing the transition between the turbid facies and the well-stratified facies. See Fig. 3.2 for profile location.

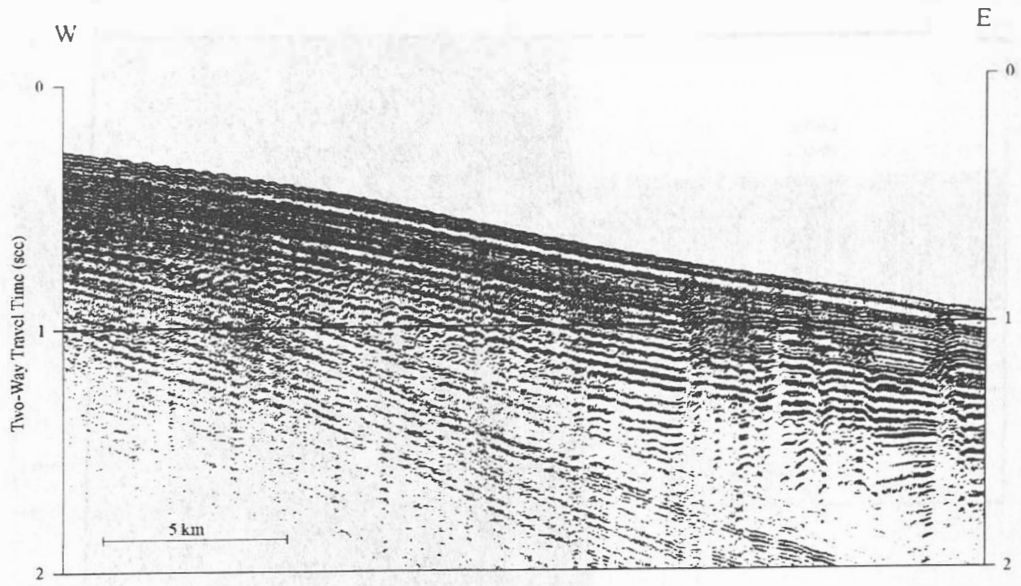

Fig. 3.7: *Part of reflection seismic profile 8 showing the well-stratified sedimentary unit SL on the basin slope within the southern seepage area. Note that the occurence of gas in the sediments leads to velocity pull-down, velocity pull-up and acoustic masking. See Fig. 3.2 for profile location.*

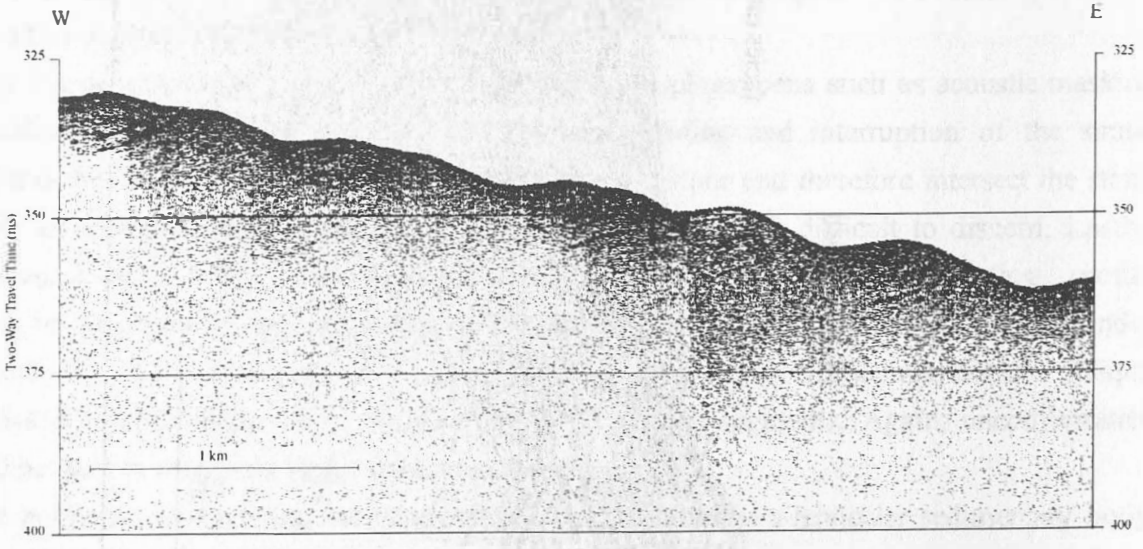

Fig. 3.8: *Part of echosounder profile 6 showing the stepwise descent of the seafloor along en echelon normal faults with small throws. See Fig. 3.2 for profile location.*

3.2 Gravity and magnetics

By S.M. Nikolaev and T. Kolpashikova

Gravity and magnetic measurements were carried out simultaneously with the seismic reflection survey. Magnetic anomalies can be calculated after the regional magnetic field and its temporal variations are subtracted from the measured field values, a process that will take place at the home laboratory in Vladivostok. Also, the gravity anomaly field will be calculated after the gravity observations at the base station in Vladivostok are completed.

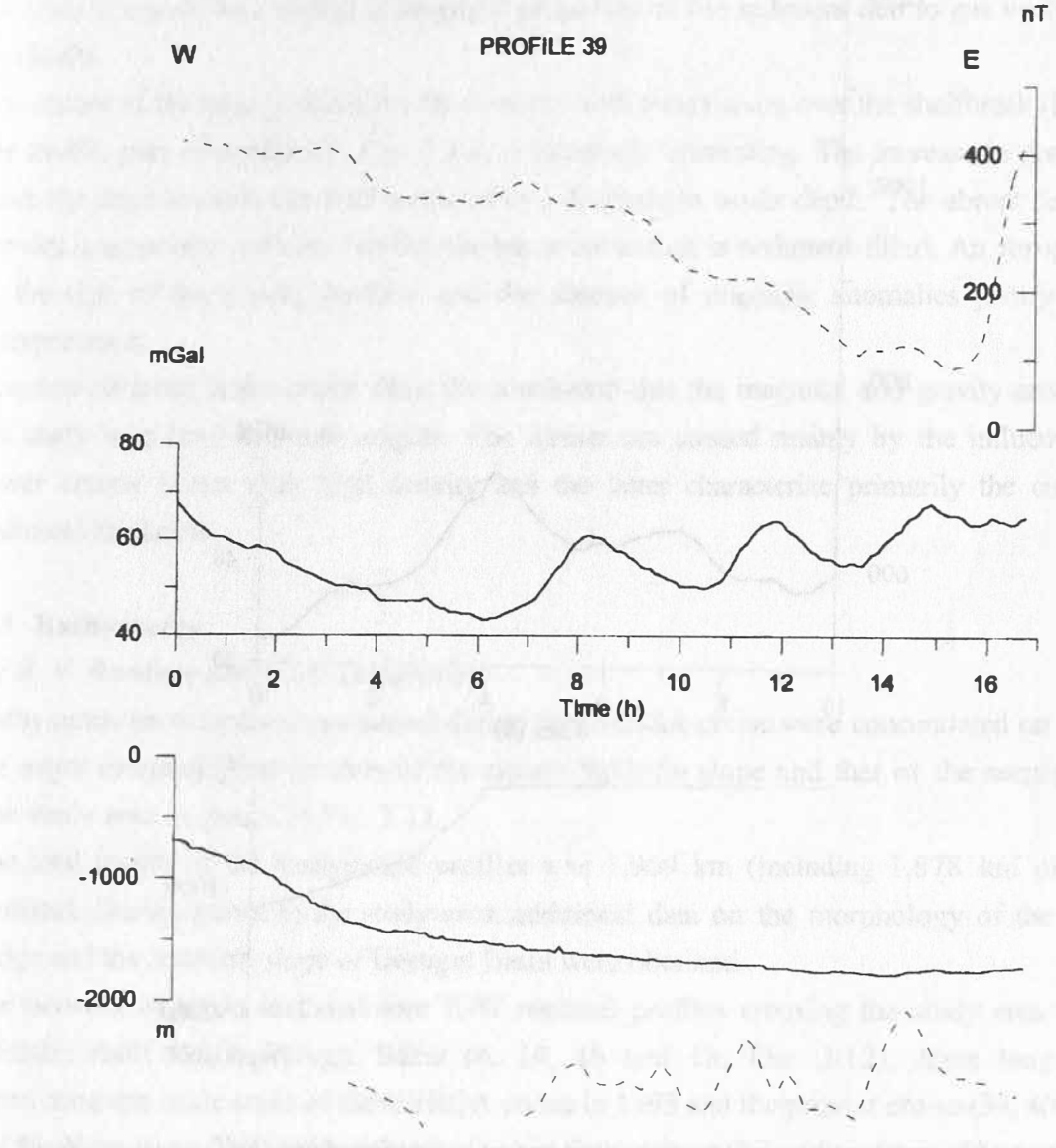

Fig. 3.9: Relative values of the gravity (solid line) and magnetic (dashed line) fields along profile 39 (top). Bathymetry (solid line) and acoustic basement (dashed line) profiles (bottom). See Fig. 3.2 for profile location.

Gravity and magnetic measurements were carried out during this cruise in the region with a thick sedimentary section, which has resulted in a sufficient decrease in anomalies connected with density and magnetic heterogeneities in the lower crustal layers. Thus, along most of the profiles, a gradual increase in geophysical fields from the deep basin in the direction of the shelf

can be observed. The increase in geophysical fields which is mainly connected with progressive shallowing is complicated by a number of minor local geophysical anomalies. They apparently are caused by crustal blocks bounded by faults or by changes in physical properties of the sediments due to gas venting along these faults.

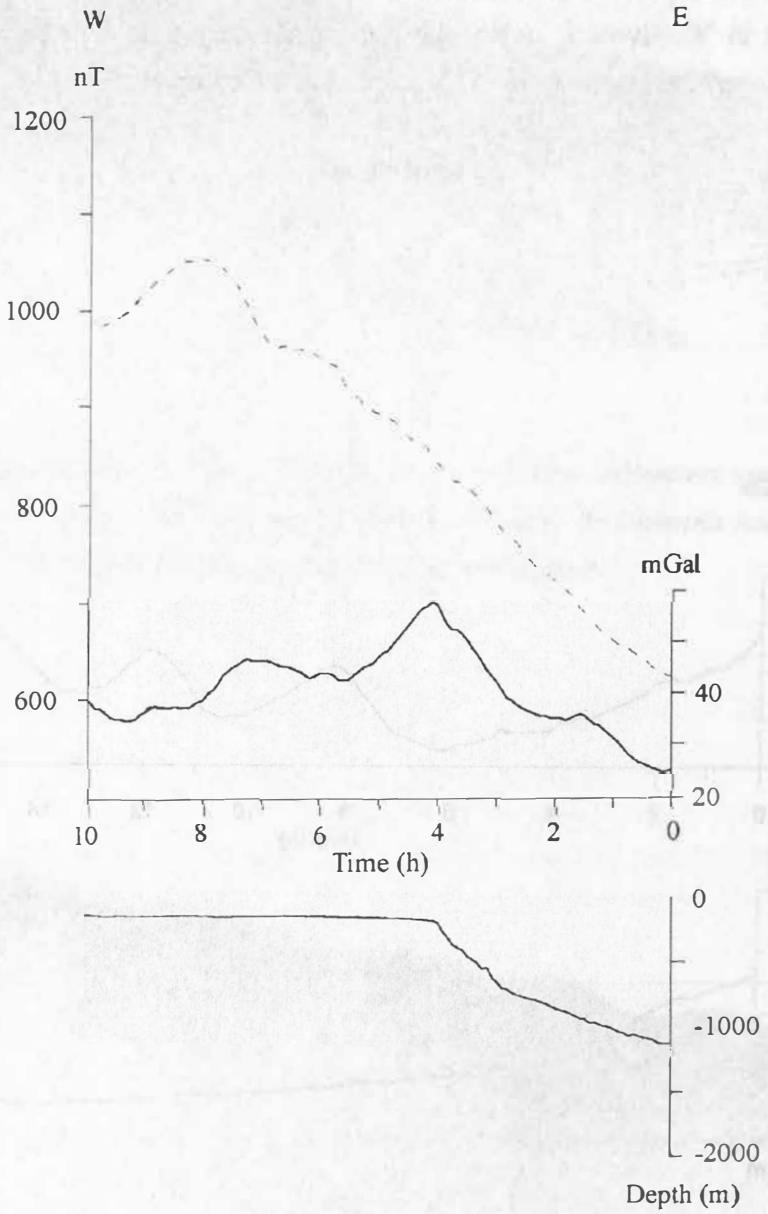

Fig. 3.10: *Relative values of the gravity (solid line) and magnetic (dashed line) fields along profile 18 (top). Bathymetry (solid line, bottom). See Fig. 3.2 for profile location.*

Two geophysical profiles with the most representative local anomalies are shown in Figs. 10 and 11. On the profile 39 (Fig. 3.9), the acoustic basement was determined and basement highs are found to coincide with large positive local gravity anomalies and weak magnetic anomalies. The latter are caused by a decrease in the thickness of the upper sedimentary layer. On the shelf

where the upper sedimentary layer is thicker, the basement high within the continental slope is marked by a positive local gravity anomaly which is not manifested in the magnetic field.

The acoustic basement trough at the end of profile 39 is poorly exhibited in the gravity field but it is represented by an abrupt increase in the magnetic field. It points to changes in the magnetic and density characteristics of the sediments here. On this profile within the continental slope, only a small local magnetic anomaly is observed. This anomaly reflects a crustal block separated by faults which are distinctly expressed in the bottom morphology. We suggest that this anomaly is caused by a change in magnetic properties of the sediment due to gas venting along the faults.

The nature of the large positive gravity anomaly with a maximum over the shelfbreak (located in the middle part of profile 18, Fig. 3.10) is extremely interesting. The increase in gravity field from the slope towards the shelf is caused by a decrease in water depth. The abrupt decrease in gravity is associated with the fact that the basement trough is sediment-filled. An abrupt change in the sign of the gravity gradient and the absence of magnetic anomalies justify such an interpretation.

The data obtained in this cruise allow the conclusion that the magnetic and gravity anomalies in the study area have different origins. The former are caused mainly by the influence of the lower crustal layers with high density and the latter characterize primarily the changes in sediment thickness.

3.3 Bathymetry

By B. V. Baranov and K. A. Dozorova

Bathymetric investigations conducted during the INESSA cruise were concentrated on mapping the major morphological features of the eastern Sakhalin slope and that of the seepage areas. The study area is shown in Fig. 3.11.

The total length of the bathymetric profiles was 1,969 km (including 1,878 km of seismic profiles). During transit to the study area, additional data on the morphology of the Polevoy Ridge and the southern slope of Derugin Basin were obtained.

The network of tracks included four E-W regional profiles crossing the study area from the Sakhalin shelf to the Derugin Basin (4, 14, 16 and 18; Fig. 3.12), three long profiles connecting the study areas of the GERDA cruise in 1995 and the present cruise (39, 40 and 41), and two sets of profiles representing surveys in the northern (N) and southern (S) seepage areas (Fig. 3.13).

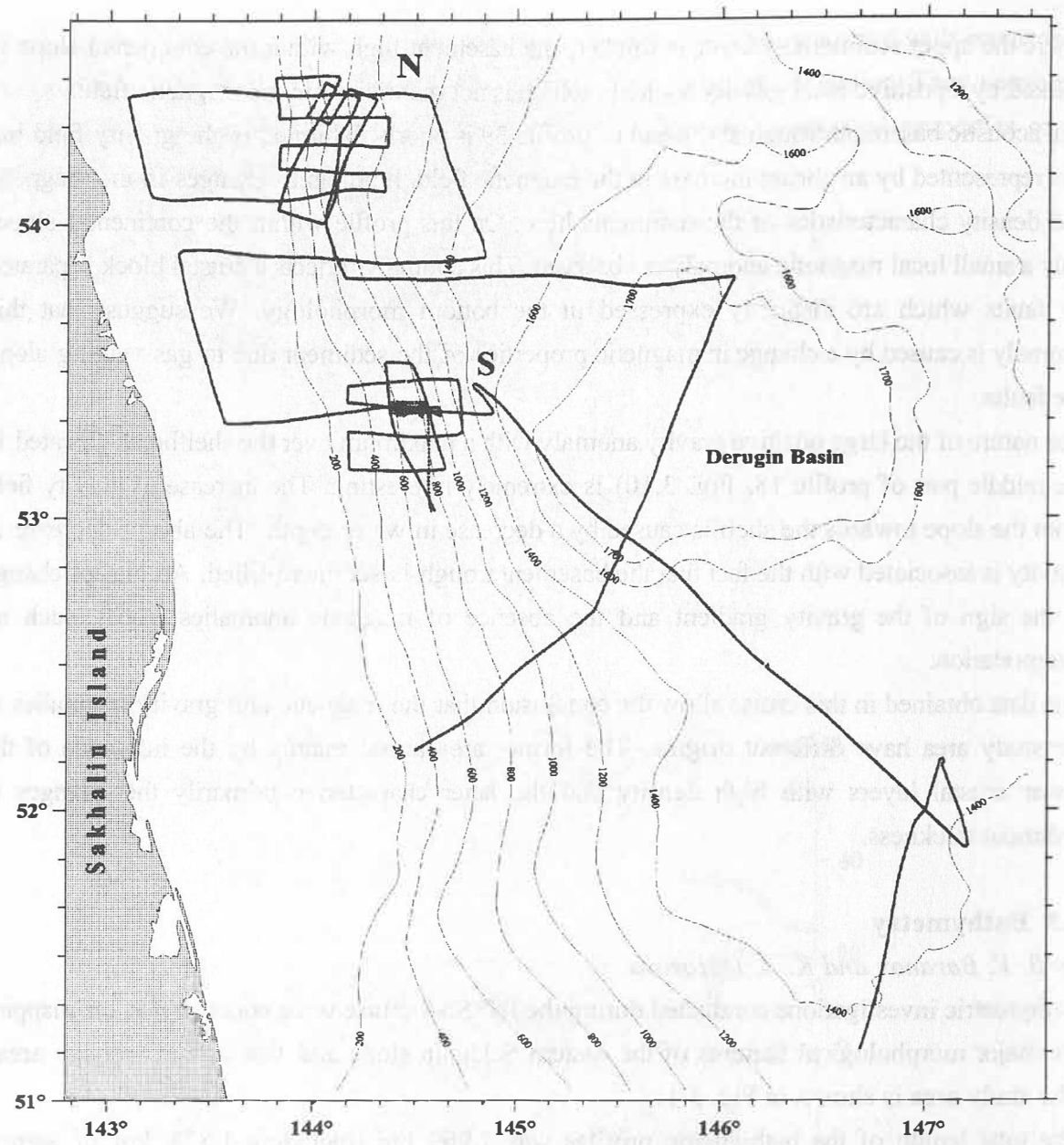

Fig. 3.11: General bathymetry and track locations within the study area. N=northern seepage area, S=southern seepage area. Contour interval is 200m.

Both of these seepage areas were covered by E-W, N-S and NNE-SSW profiles with lengths of 20-60 nm some 5-10 nm apart organized in a semi-regular network. In addition, a small region within the southern seepage area was covered by a dense net of echosounder profiles with a spacing of 0.5-1 nm. The same coverage was used during a previous cruise of the *RV Andropov* for the northern seepage area (Ginsburg et al., 1993).

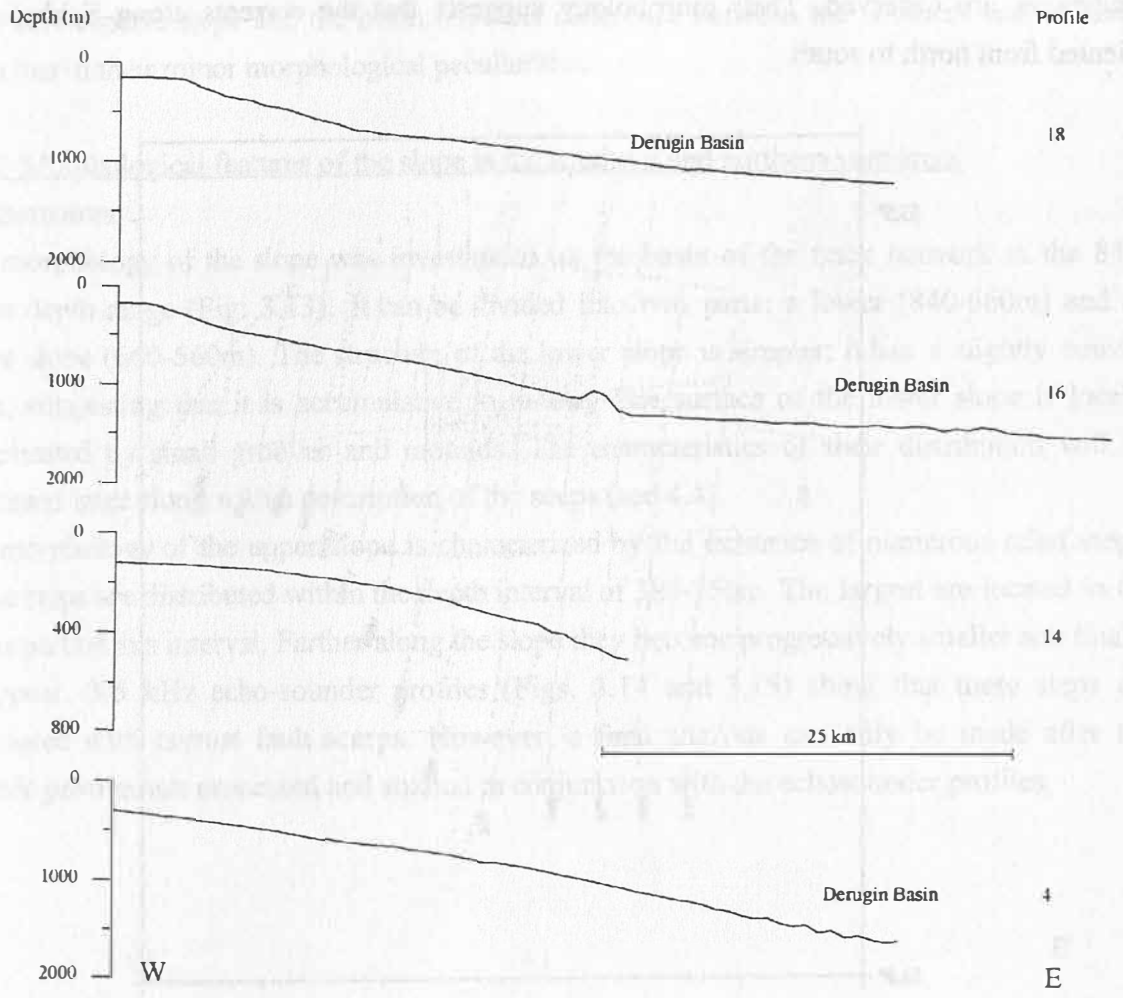

Fig. 3.12: *Bathymetric profiles across the Sakhalin slope showing the morphology of the southern (profiles 4 and 14) and northern (profiles 16 and 18) areas.*

3.3.1 The east Sakhalin continental slope

During the INESSA expedition, the continental slope was covered by profiles at a spacing of 90 nm between 53°N and 54.5°N (Fig. 3.11). Within this study area, as can be seen on the GEBCO bathymetric map, the slope has a near-meridional strike (NNW, 350°). However, on separate minor transects, the slope is found to stretch in a zigzag manner in the NNE (10°) direction in general.

Regional profiles (4, 14, 16 and 18) shown in Fig. 3.12 demonstrate the structure of this slope. Clearly, the slope morphology is in general extremely simple and changes only slightly from south to north. In the northern part of the study area, the shelfbreak is very distinct and can be traced at depths between 170-180m (profiles 16 and 18). In the south, the shelfbreak is less distinct and two steps are evident: the first is located at 200-210m and the second at 130-135m. Landwards of the shelfbreak lies the shelf which is represented by a eastward sloping plain within the depth range of 180-50m. On profile 15 which transects the shelf in a N-S direction,

sandwaves are observed. Their morphology suggests that the currents along Sakhalin are oriented from north to south.

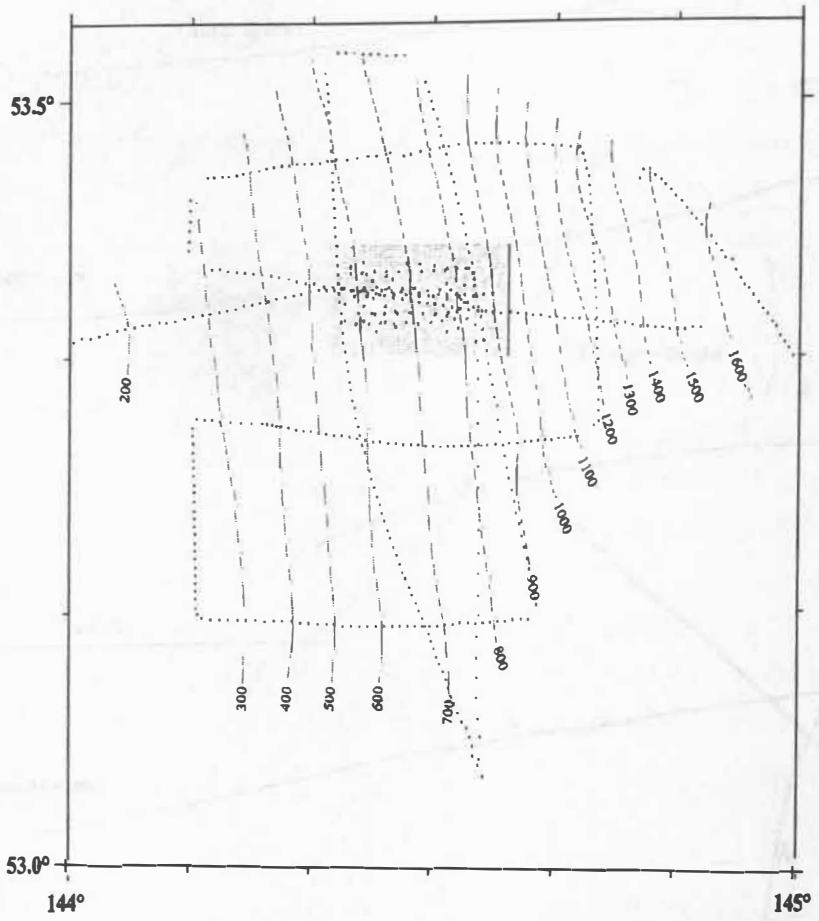

Fig. 3.13: Bathymetry of the southern area. Contour interval is 100m. Dotted lines show tracks, rectangle indicates detailed area shown in Fig. 3.8.

The continental slope in the southern part of the study area is in general more gentle (1.5°) compared to the north (2.5°). As a result, the shelf width is approximately equal to the slope width in the southern area but exceeds it by a factor of two in the north. The slope morphologies also differ. In the southern part of the area, it has a convex profile and an additional gentle step within the depth range from 500-600 to 700-800m. In contrast, the slope of the northern area has a concave profile with an upper slope gradient of 4-5° and a depth range reaching from the shelfbreak to 400-500m.

Our bathymetric survey shows that the transition from the continental slope off Sakhalin to the Derugin Basin floor may be smooth but may also consist of several steps. On profile 16 (Fig. 3.12), the seafloor gradient changes twice, viz. at the depth intervals of 1150-1300m and 1400-1480m respectively. Farther seawards lies the abyssal plain. A second example is given by profile 4 (Fig. 3.12) in which a series of highs of up to 50m above the surrounding seafloor

exist between the slope and the basin. Another difference between the southern and northern areas lies in their minor morphological peculiarities.

3.3.2 Morphological features of the slope in the southern and northern vent areas

Southern area:

The morphology of the slope was investigated on the basis of the track network in the 840-560m depth range (Fig. 3.13). It can be divided into two parts: a lower (840-660m) and an upper slope (660-560m). The structure of the lower slope is simpler; it has a slightly convex form, suggesting that it is accumulative in nature. The surface of the lower slope is locally complicated by small grooves and mounds. The characteristics of their distribution will be discussed later along with a description of the seeps (see 4.4).

The morphology of the upper slope is characterized by the existence of numerous relief steps. These steps are distributed within the depth interval of 380-750m. The largest are located in the upper part of this interval. Farther along the slope they become progressively smaller and finally disappear. 3.5 kHz echo-sounder profiles (Figs. 3.14 and 3.15) show that these steps are associated with normal fault scarps. However, a final analysis can only be made after the seismic profiles are processed and studied in conjunction with the echosounder profiles.

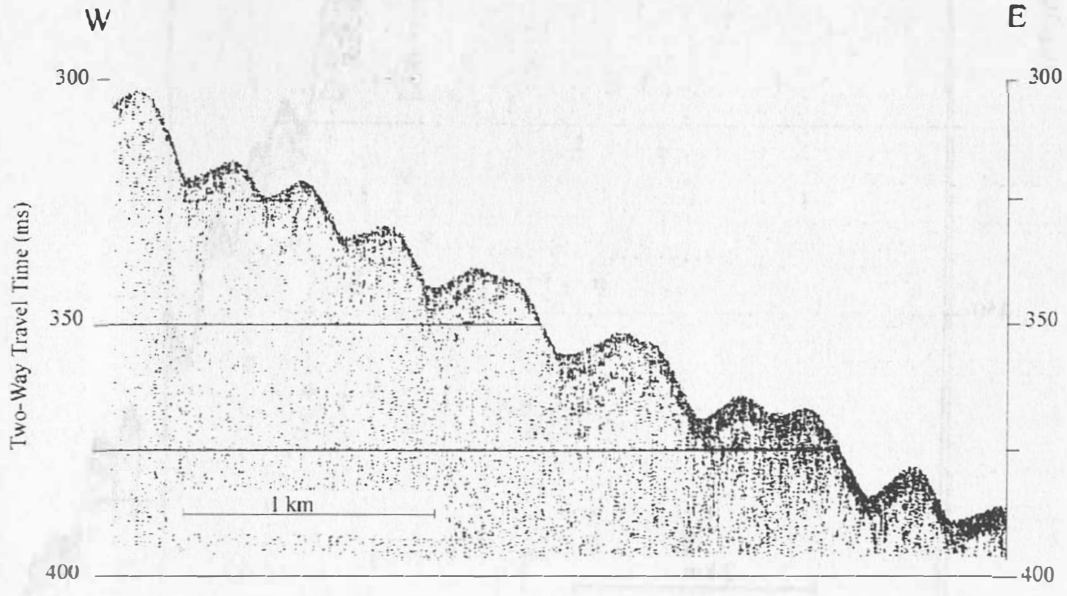

Fig. 3.14: 3.5 kHz echosounder record showing step-like morphology of the upper slope (southern area). Part of profile 14.

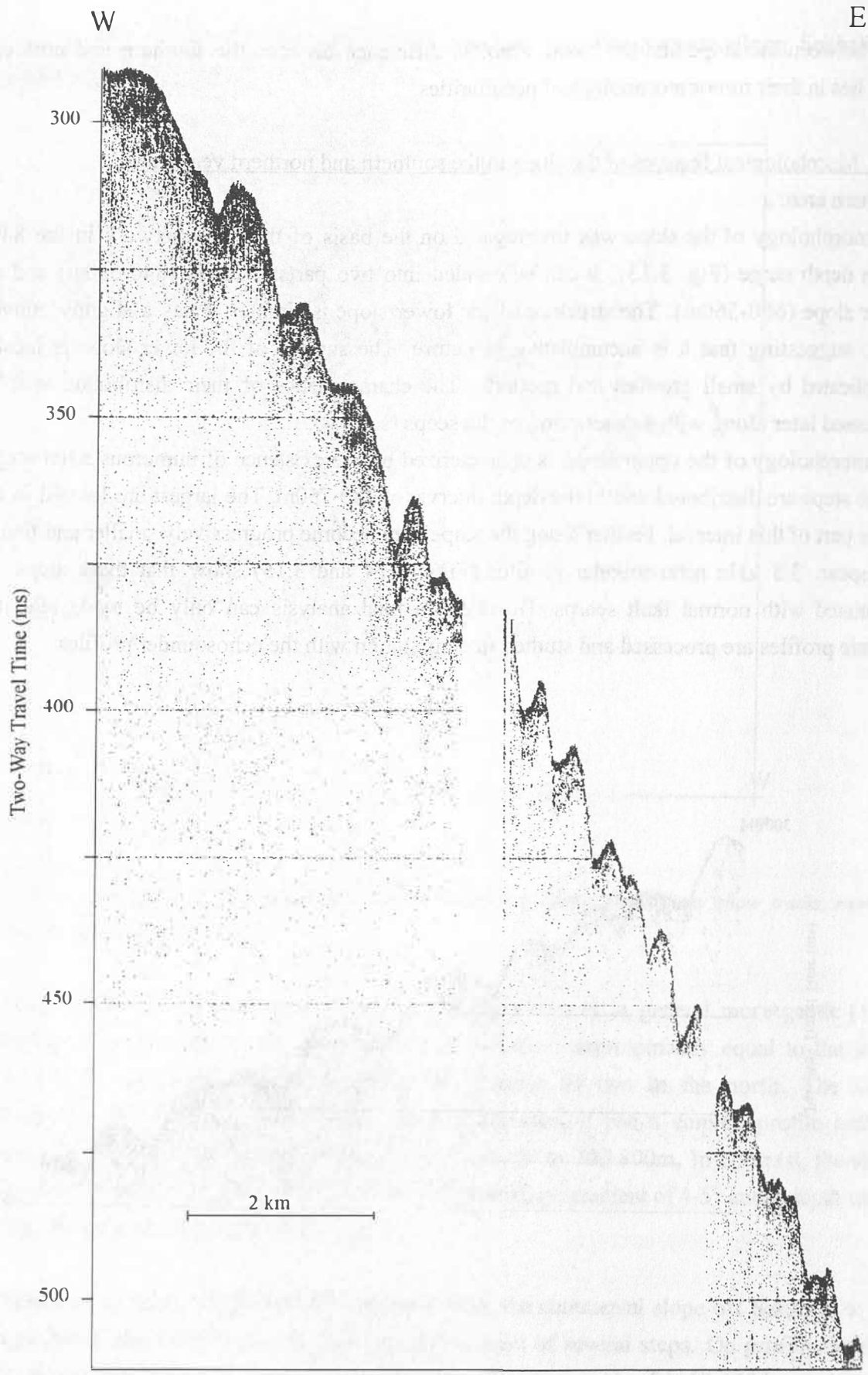

Fig. 3.15: *3.5 kHz echosounder record showing step-like morphology of the upper slope (southern area). Part of profile 10.*

Northern area (Fig. 3.16):

Data obtained from the northern area show that the slope morphology here is different from that to the south. The zone from the shelfbreak down to a water depth of 900-950m was studied in the northern area. Between the shelfbreak and 680m depth, the seafloor is steeper than at greater depths. Sometimes it has a step-like structure, but the morphology of the steps here contrasts sharply with that in the southern area. Firstly, the gradient is gentler and secondly their steep sides face upslope while their gentle sides face downslope.

The 3.5 kHz echosounder records permit a determination of the displacement character on these steps (Fig. 3.17). On profile 16 which lies in the north (according to its relief), the step-like structures can be observed at depths of 430-540m. It can be clearly seen that the steps are made up of deformed sediments. Structures reminiscent of drag folds are also present. Deformations have also been observed within the upper sedimentary column on other profiles crossing the northern area.

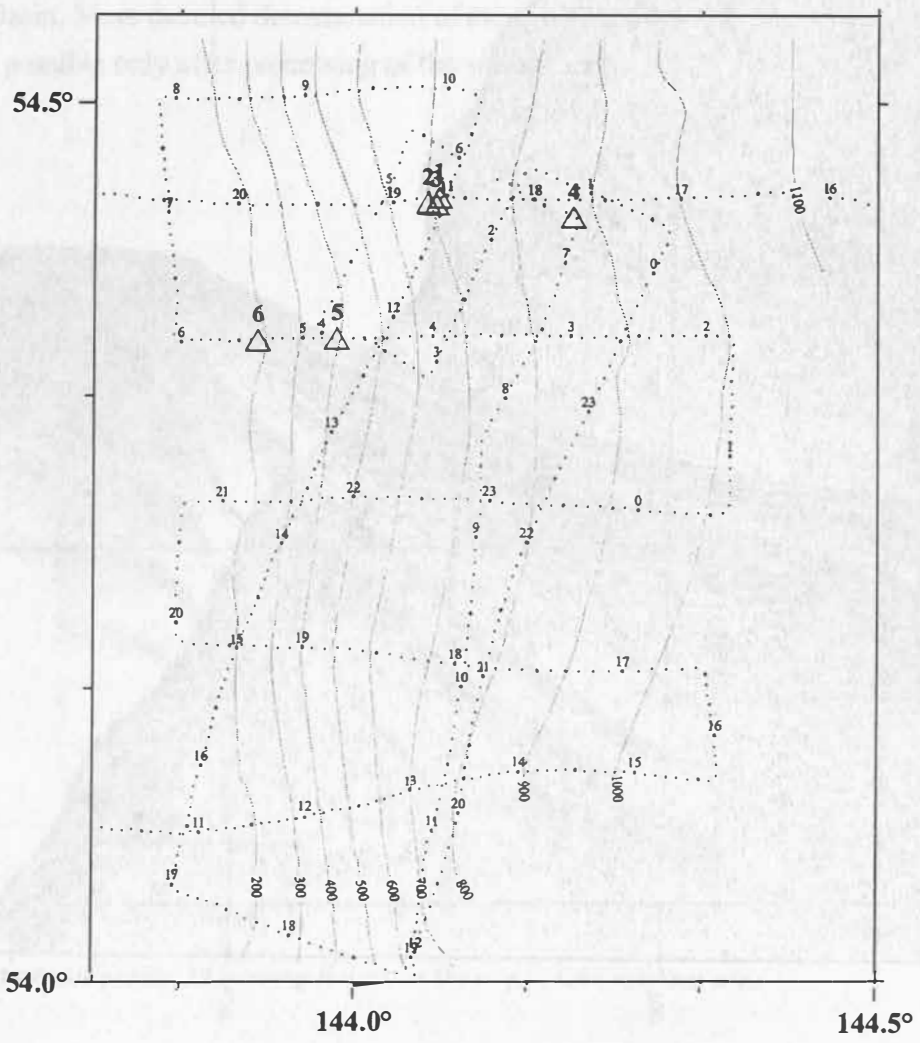

Fig. 3.16: Bathymetric map of the northern area. Dotted lines indicate tracks, numbers give the time (UTC). Triangles mark seeps with numbering after Ginsburg et al. (1993).

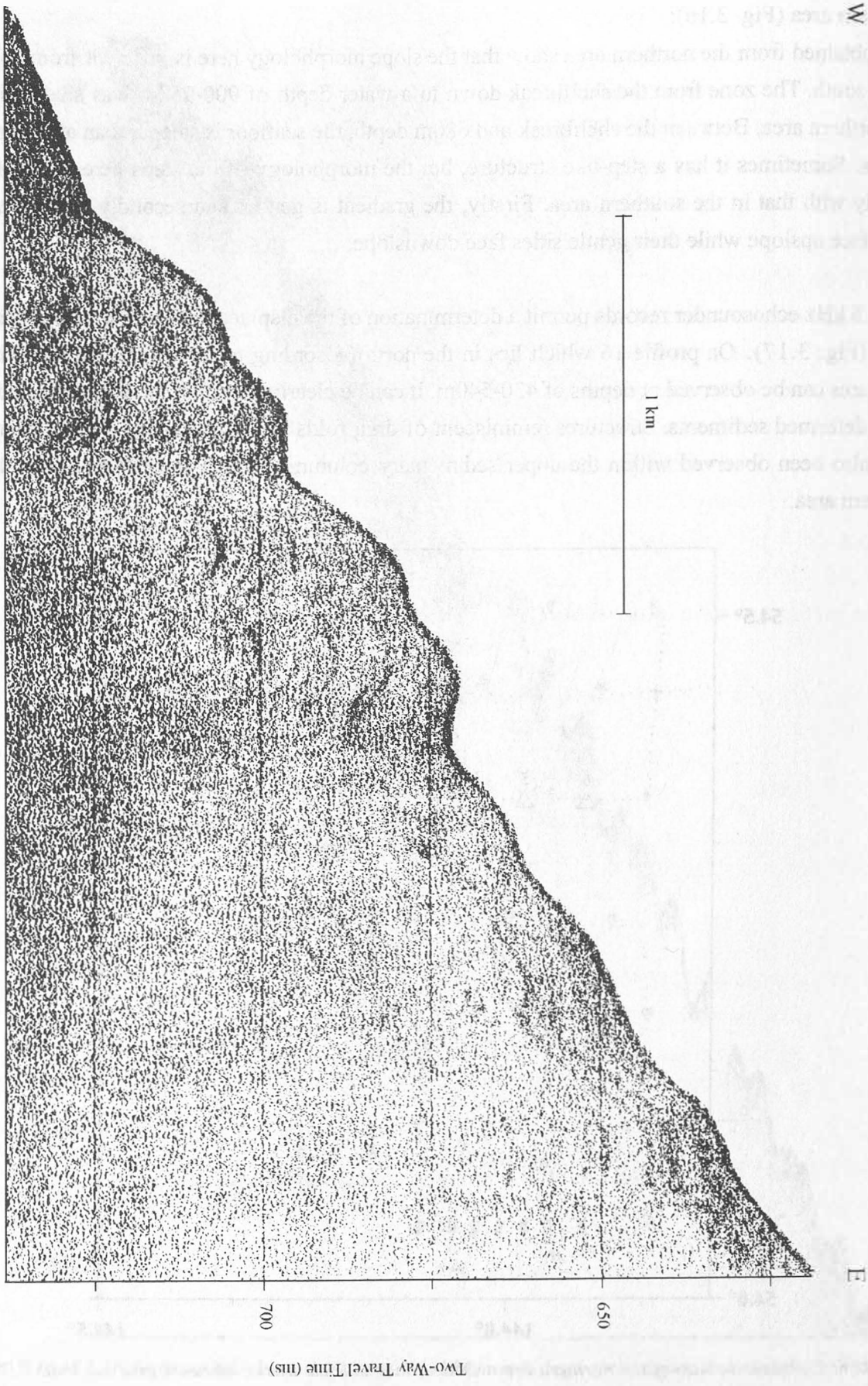

Fig. 3.17: Compressional structures on the slope of the northern area. Part of profile 16, 3.5 kHz record.

4. DISCUSSIONS

4.1 Tectonic structure of the INESSA area

By B. V. Baranov, B. Ya. Karp, H. K. Wong, T. Lüdmann, and K. A. Dozorova

Gnibidenko and Svarichevsky (1984) and Ginsburg et al. (1993) published their concepts on the systems of ancient and recent faults on the eastern Sakhalin slope. For example, they suggested the existence of a large, north-south striking rupture zone separating Sakhalin Island from the Derugin Basin. However, the tectonic nature of this zone remains obscure. Two fault systems oriented NNW and NNE have also been recognized in this region.

Tectonic data obtained during the INESSA expedition permit the formulation of a new approach to this question. The most interesting data were collected from the northern seepage area. All seismic profiles from this area show numerous stratal offsets. According to the displacement character of the reflectors, these offsets can be interpreted to mark reverse faults and thrusts (Fig. 4.1). Some of them appear to dip towards the continental slope while others dip towards the Derugin Basin. More detailed determination of the dip azimuths as well as the nature of the faults will be possible only after processing of the seismic data.

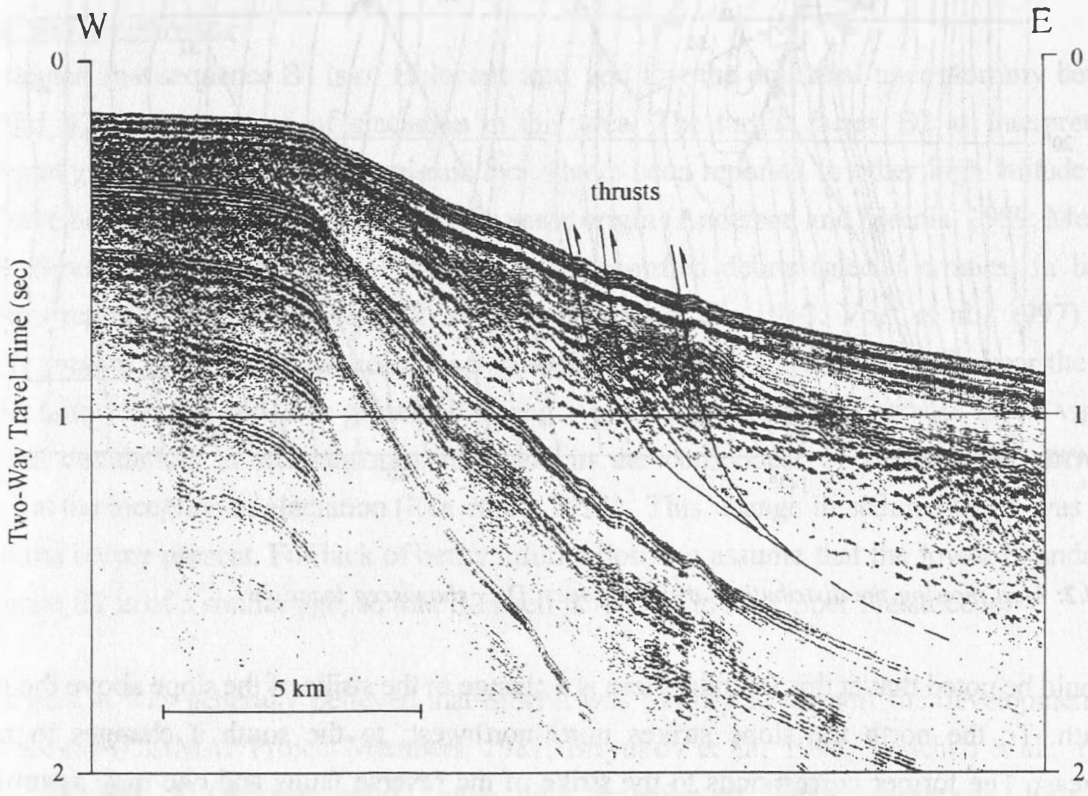

Fig. 4.1: *Part of seismic profile 28 showing thrusts on the slope of the northern area.*

In the northern area and on two profiles to the south, the main faults can be well-correlated across profiles so that their strikes (in the NW and NNW directions) can be inferred. Near the

northern seeps, these faults are concentrated in two zones (Fig. 4.2): upslope where the bottom gradient is particularly steep beginning at 700m water depth, and downslope starting from 800m depth. The abundance of these faults decreases to the south. They are widespread in the northern part of the area, but cease to exist south of about 54°22'N.

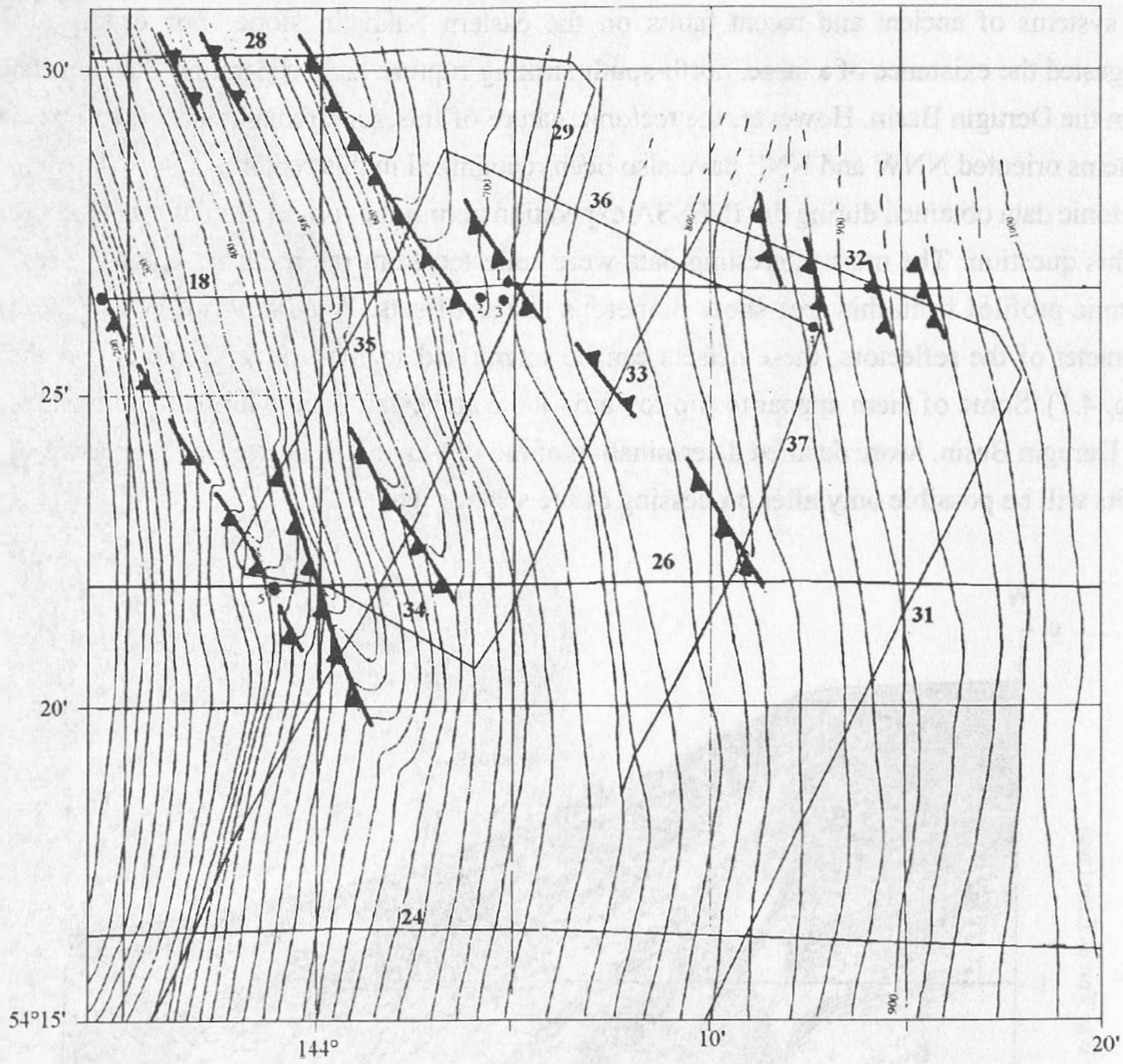

Fig. 4.2: Map showing the distribution of thrust zones. Dots show seep locations.

It should be noted that at this latitude, there is a change in the strike of the slope above the 600m isobath. To the north the slope strikes north-northwest; to the south it changes to north-northeast. The former corresponds to the strike of the reverse faults and one may assume that the latter gives the strike of the second fault system which is possibly strike-slip. We will return to this question again later. It suffices to note that the gradual disappearance of reverse faults towards the southeast implies that an orthogonal system of faults exists here and that these faults must in such a case be strike-slip. Faults within this reverse fault system form typical steps on the upper part of the slope and gentle scarps on its lower part.

The tectonic style of the southern seepage area is not very obvious. It should be noted that reverse faults that are widespread in the northern area are absent on seismic profiles from the south. Nevertheless, step-like relief on the upper slope is better manifested here. However, it is not possible to draw any conclusions on the type of displacements responsible for this morphology from the seismic profiles or from the 3.5 kHz echosounder records. On the echograms, such features look very similar to a series of normal fault scarps (see Figs. 3.14 and 3.15) although similarities to a system of reverse fault steps are present on some profiles.

The tectonic style of the eastern Sakhalin continental slope changes significantly from north to south. In the north, it is governed by a system of NNW- to NW-striking thrusts and reverse faults which governs the slope morphology. We can assume the existence of NNE-oriented strike-slips here. In the south, the faults are less well seismically expressed. They may show vertical displacements but are not correlatable with each other. Thus, one may conclude that the main displacements here are represented by strike-slips.

4.2 Seismo-stratigraphy and paleo-depo-environment

By H. K. Wong, B. Ya. Karp, B. V. Baranov, and T. Lüdmann

4.2.1 Basinal province

We suggest that sequence B1 is of Holocene age, and that the erosional unconformity between B1 and B2 marks the end of glaciation in this area. The turbid facies B2 is interpreted to represent glacial deposits. Similar seismic facies have been reported in other high latitude areas and have been attributed to sediments of the same origin (Anderson and Molnia, 1989; Menzies, 1995; Syvitski et al., 1997). The abundance of ice-rafted debris (glacial erratics) in bottom samples reported from the Derugin Basin (Gorbarenko et al., 1990; Vogt et al., 1997) lends further support to this interpretation. Deep sea drilling in the northwestern Pacific near the Meiji Guyot (site 192, leg 145) has presented strong evidence for a sudden increase in the vigor of deepsea circulation, in sedimentation rate, and in the component of fine-grained terrrestrial debris at the inception of glaciation (Rea et al., 1993). This change in sedimentation was dated at 2.6 ma before present. For lack of better information, we assume that the lower boundary of sequence B2 is of a similar age, so that B2 itself is formed in the Upper Pleistocene.

In the past, it was generally believed that Siberia was too dry to support the development of a large ice cap (CLIMAP Project Members, 1981; Biryukov et al., 1998; Velichko et al., 1993). Thus, the Sea of Okhotsk would have only experienced minor glaciations during the Pleistocene. Recent evidence, including computer model simulations, however, suggests that a Pleistocene highland ice sheet probably developed over the North Pacific Rim and spilled over into the Sea of Okhotsk (Hughes, 1995; Grosswald, in press; Grosswald and Hughes, 1998). During the stadials, ice could have advanced as grounded ice over the northern shelf, and

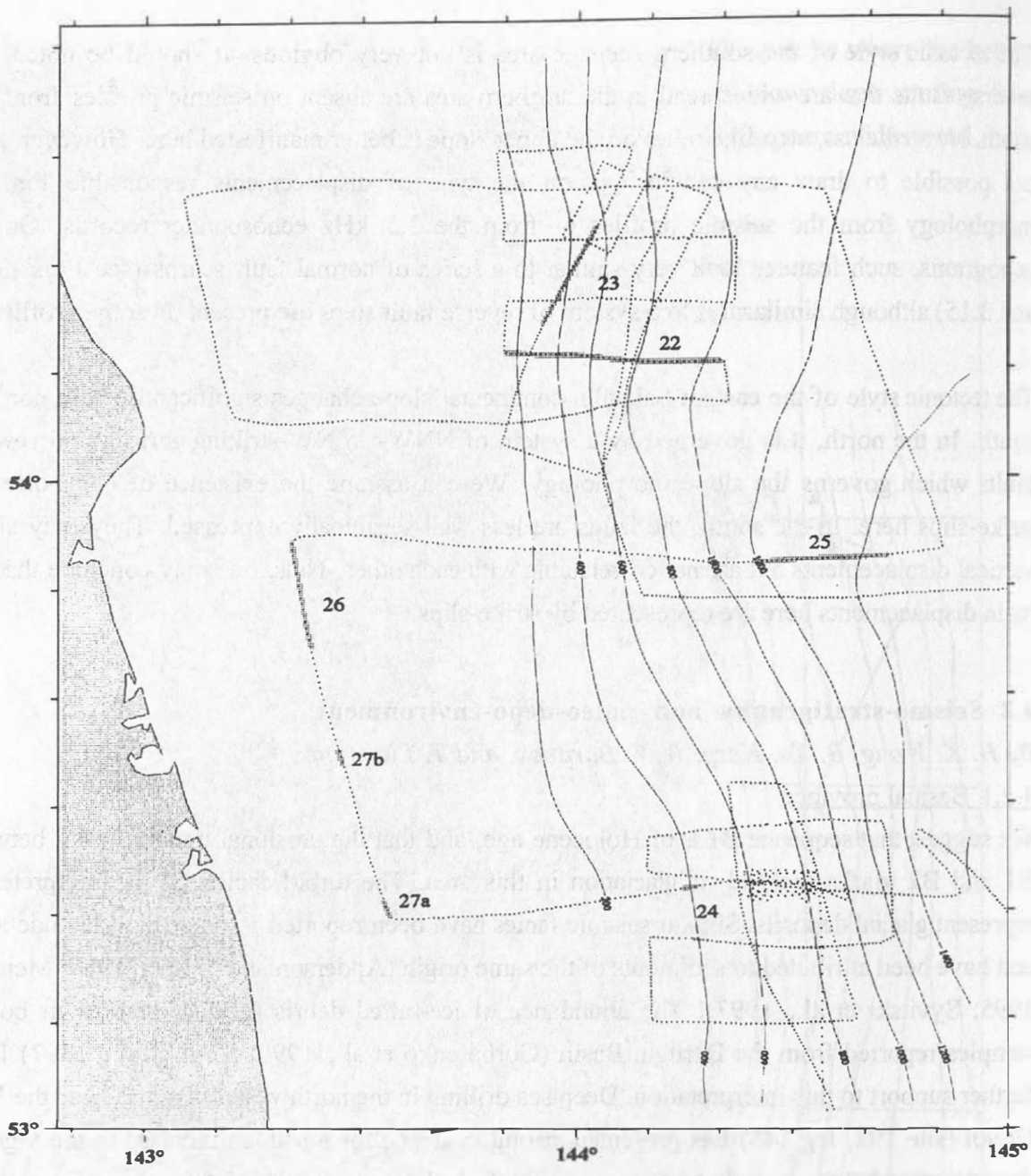

Fig. 4.3: Location of the selected profiles shown in Figs. 4.4-4.10.

continued as floating ice southwards, ending as a calving ice front along the Kurile Islands which acted as a pinning point. During interstadials, the ice front probably retreated to the northern shelf of the Okhotsk Sea. If this scenario is assumed to be qualitatively true, then a large amount of glacial sediments must have been transported over and deposited in our study areas, although the depositional pattern would be difficult to predict because the location of the ice front and its changes through time as well as the accompanying changes in the drainage systems, especially that of the Amur, cannot be readily reconstructed. However, the tongue-like extension of area II northwards onto the basinal slope suggests that ice advance from Sakhalin Island into the Derugin Basin must have played an important role in shaping the glacial sediment distribution pattern.

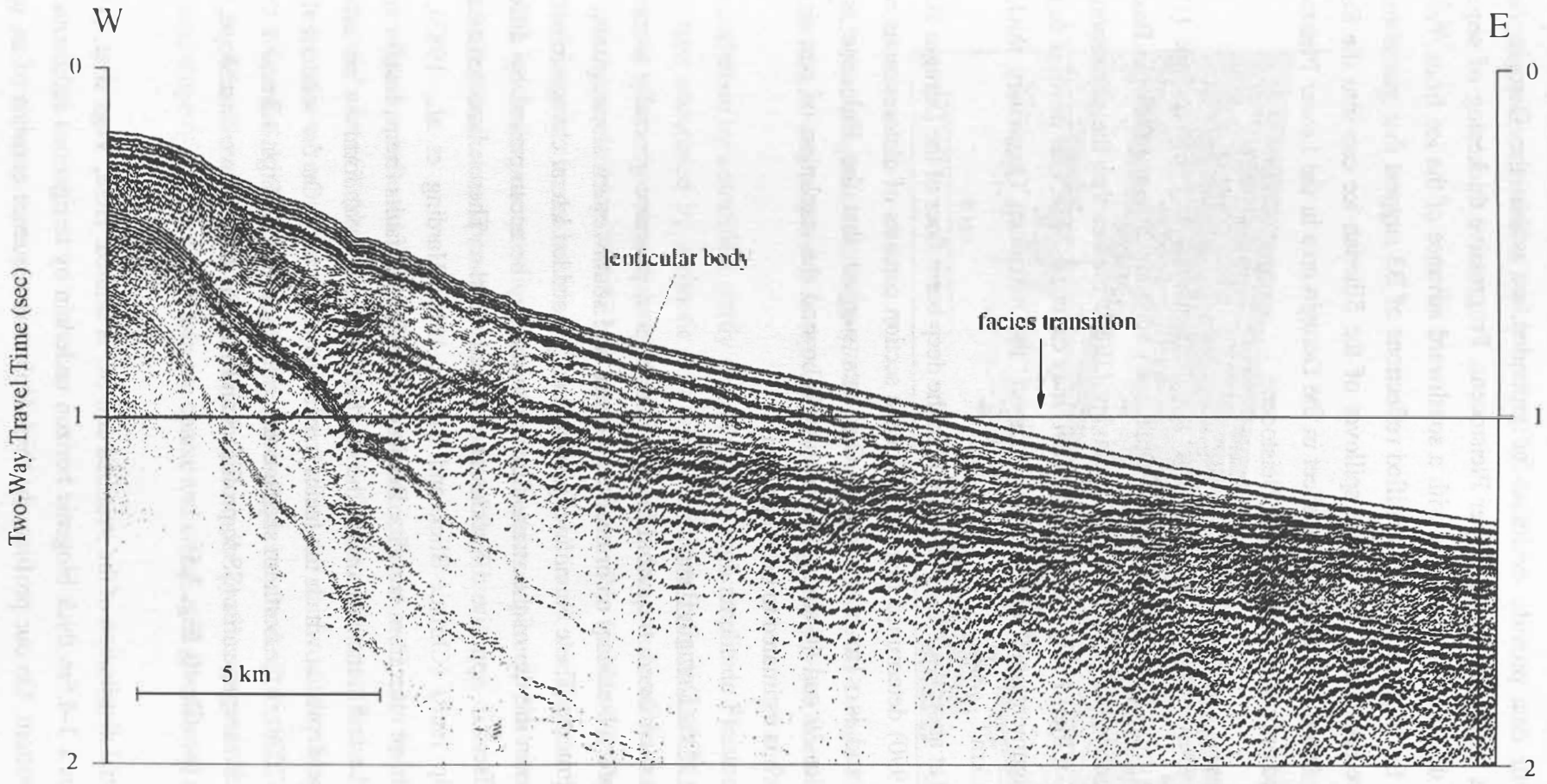

Fig. 4.4: *Reflection seismic profile 22 within the northern seepage area showing a lenticular, semi-transparent sedimentary body comprising two subsequences. See text for explanation. Note that the turbid facies grades abruptly to a well-stratified facies. See Fig. 4.3 for lacation.*

The turbid internal configuration of sequence B2 precludes its interpretation as glacial-marine sediments. Thus, our data provide evidence for grounded ice within the Derugin Basin, including its deepest parts, during the Upper Pleistocene. Progressive thickening of sequence B2 in the southerly direction is consistent with a southward advance of the ice front. Prior to this time, however, the high amplitude, stratified reflections of B3 suggest that glacial-marine conditions must have prevailed. That is, the spillover of the Siberian ice cap into the Sea of Okhotsk must have started as a floating ice sheet in the Derugin area in the Lower Pleistocene and became grounded only later in the Upper Pleistocene.

The sequences B4 to B6 are pre-Pleistocene in age. Gnibidenko and Khvedchuk (1982) reported that the maximum thickness of the Plio-Quaternary section within the Derugin Basin is about 1 km. In contrast, the profile I-I' of Zhuravlev (1984) implies that the corresponding thickness (thickness of their Pomyzskoe seismic unit) may exceed 1.2 km. Our profiles suggest that, if our age assignments are approximately correct, the maximum Quaternary thickness would reach about 1 km.

Using a core located at about 54.1°N, 146.3°E within the deep basin floor of the Derugin Basin, Gorbarenko et al. (1990) determined that the Holocene section consists of diatomaceous ooze, fine silt and pelite and is <1m in thickness. Our data suggest that the Holocene at the intersection of profiles 39 and 40 about 45 km away is beyond the resolution of our air gun seismic system, which is estimated to be about 15m.

4.2.2 Western slope of the Derugin Basin

As has already been mentioned, the turbid facies of the basinal province generally terminates abruptly at a sharp, steep boundary on or near the western and southwestern slope, giving way to well-stratified sediments. These boundaries mark not only a sudden lateral change in seismic facies, but often also in the dip of the strata. Such changes may be accompanied by different stratal offsets or offsets in opposite directions at different depths. These characteristics are typical for strike-slip faults (Christie-Blick and Biddle, 1985; Harding et al., 1983), the occurrences of which we infer from our data. Because the strike-slip faults (transpressive in the northern seepage area and transtensional in the southern seepage area) form an en echelon system (see 1.1), the depths at which the facies transitions occur vary. On the western slope, they range between 700m in the northern seepage area (NSA, profile 22, Figs. 4.3 and 4.4) and 1,500m in the southern seepage area (SSA, profiles 8 and 10). On the southwestern slope, they are at about 1,600m (profile 40, Fig. 3.5).

At the NSA, the spatial distribution of the stratified unit SL is limited. Here, Vogt et al. (1997) reported from 4 cores a 1-4.5m thick biogenic horizon underlain by terrigenous sediments that extend to the core bottom. On our profiles, the thick Holocene sequence consists of an upper

subsequence conformal to the seafloor and a lower, stratified to semi-transparent, truncated subsequence that terminates toplap updip (Fig. 4.4).

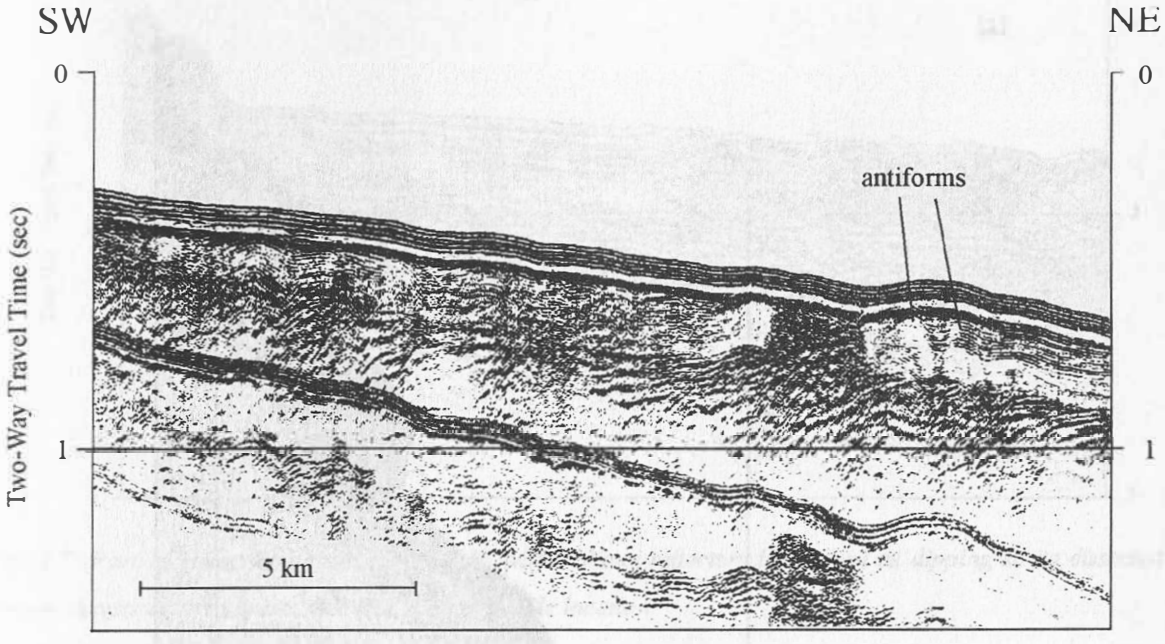

Fig. 4.5: Part of reflection seismic profile 29 from the upper slope of the Derugin Basin within the northern seepage area showing antiforms in the Holocene section. See Fig. 4.3 for profile location.

It is underlain by a stratified, partly discontinuous, high amplitude Pleistocene sequence which is in turn succeeded by a chaotic unit with intermittent reflections. On the upper slope, the Holocene section becomes more transparent although compressional features such as antiforms with their axes striking NW-SE are sometimes discernible (profile 29, Fig. 4.5). The base of the Holocene is a marked erosional unconformity. All in all, the upper slope here is dominated by this lenticular, compressionally deformed, semi-transparent, Holocene sedimentary body which we interpret to represent fluvial deposits of the River Amur.

Generally, it is believed that during the Holocene, fluvial sediments from the River Amur are transported east of Sakhalin southwards. Part of these sediments fill the Derugin Basin, while the remainder are subsequently deposited at a site to the south to form a large sedimentary apron east of central Sakhalin. The large reflectances (high amplitudes), the lack of echo prolongation and the limited penetration on 3.5 kHz echosounder profiles suggest that sediments on the western slope of the Derugin Basin are coarse and compacted (profile 14, Fig. 4.6).

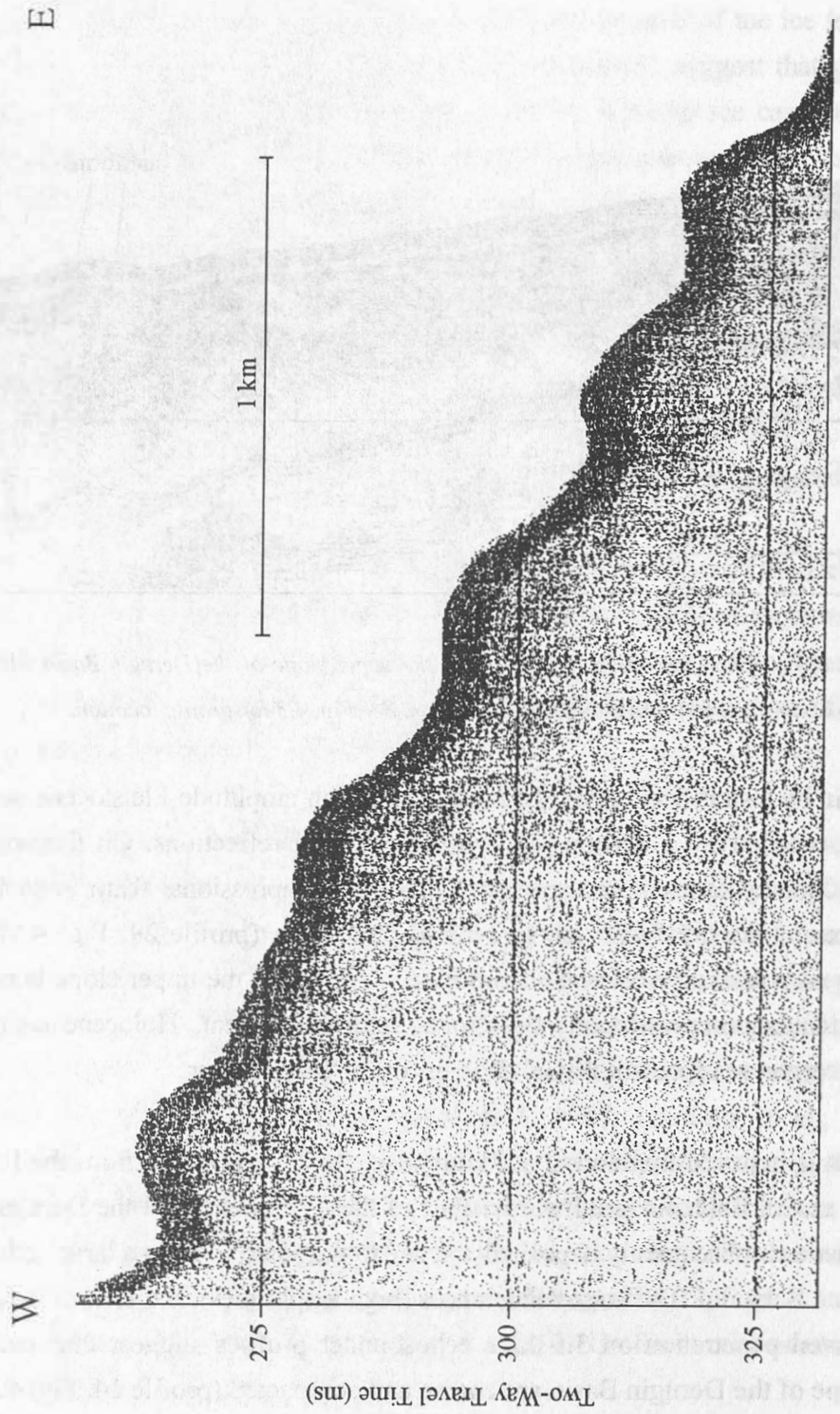

Fig. 4.6: *Part of echosounder profile 14 showing a high reflectance seafloor characterized by a lack of echo prolongation and limited penetration. See Fig. 4.3 for profile location.*

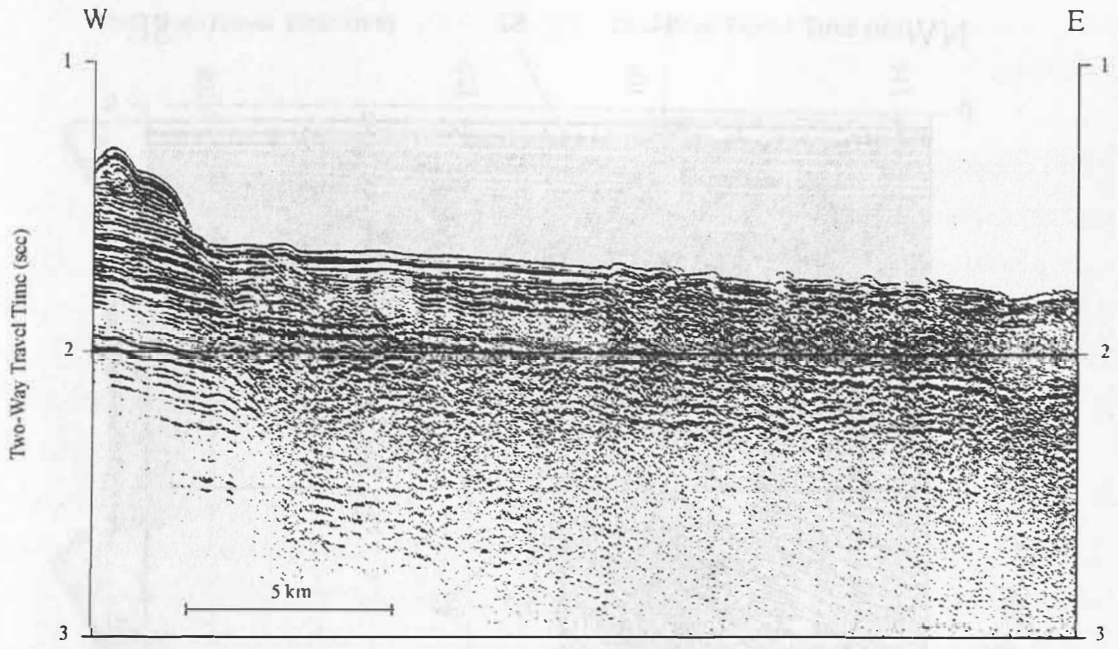

Fig. 4.7: Part of reflection seismic profile 16 with oblique reflectors interpreted as dipping strata dissected by steeper thrusts or overthrusts. See Fig. 4.3 for profile location.

Either the fine fraction is winnowed out, or it is deposited largely in the apron. Evidence for the former can be found in the correlation of the locations of the gas vents in the SSA with those of the methane anomalies in the surface waters. The southwestward displacement of the methane anomaly maximum with respect to the vents (see 4.3) suggests that there are significant currents flowing up the western flanks of the Derugin Basin from a northeasterly direction. This direction is also consistent with the NW-SE orientation of stripes of high and low backscattering strength mapped on sidescan profiles in this area. These currents may be responsible for the winnowing. If, however, only the coarse fraction is deposited on the western slope and the fine fraction is confined largely to the sedimentary apron, then the amount of sediments carried into the Sea of Okhotsk by the River Amur must be exceedingly large (52×10^6 t/a; Milliman and Meade, 1983).

Within the turbid facies at the western part of the NSA (profiles 16, 18, 20; Fig. 4.7) are correlatable, northwesterly dipping, partly continuous reflectors which probably represent dipping strata dissected by steeper thrusts or overthrusts. The fault trace of these thrusts can be reconstructed at locations where two or more of the prominent, flat-lying stratal interfaces at different depths are offset.

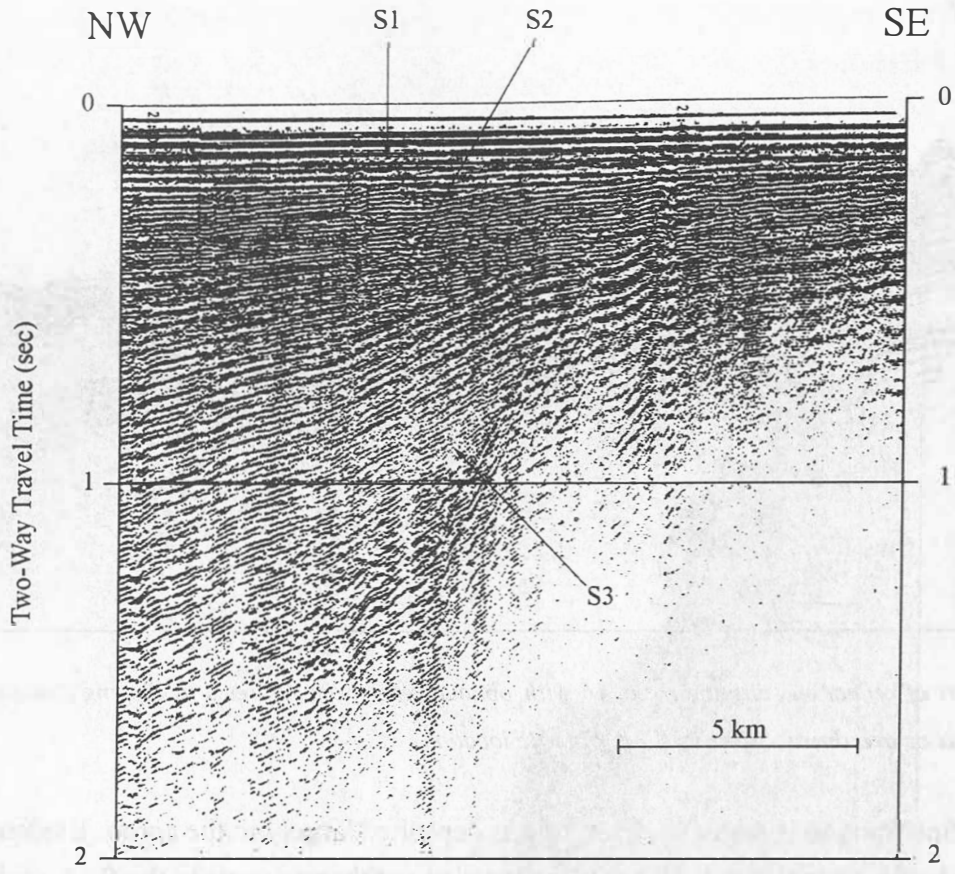

Fig. 4.8: Part of reflection seismic profile 15 which crosses the southern part of the East Shmidt Trough showing the upper basinal sequences S1 to S3. See Fig. 4.3 for profile location.

4.2.3 East Sakhalin shelf

The East Sakhalin shelf within our study area is dominated by the East Sakhalin Basin, which is separated into two subbasins by the Schmidt anticlinal zone (Gnibidenko and Khvedchuk, 1982). The western subbasin (the Piltun-Chaivinsk Trough) has a Neogene thickness (to the top of the metamorphosed Upper Cretaceous basement) of 5-9 km (Alperovich and Chernyavsky, 1973), while the corresponding value for the eastern subbasin (the East Schmidt Trough) is >7 km (Margulis et al., 1979).

Profile 15 subparallel to the Sakhalin shelf crosses the two subbasins of the East Sakhalin Basin. It shows that the Schmidt anticline is bounded by steep faults and that the basinal sediments penetrated can be divided into 3 sequences (Fig. 4.8). The lowermost sequence S3 comprises subparallel, large amplitude reflectors of low frequency and high continuity. The middle sequence S2 is a basinal fill which onlaps S3 in the south and downlaps it in the north. It probably represents fluvial-glacial sediments of the Pleistocene. The uppermost sequence S1 consists most likely of Holocene fluvial deposits derived from the River Amur. Both sequences S1 and S2 diverge and therefore thicken to the north, suggesting an increase in distance to the

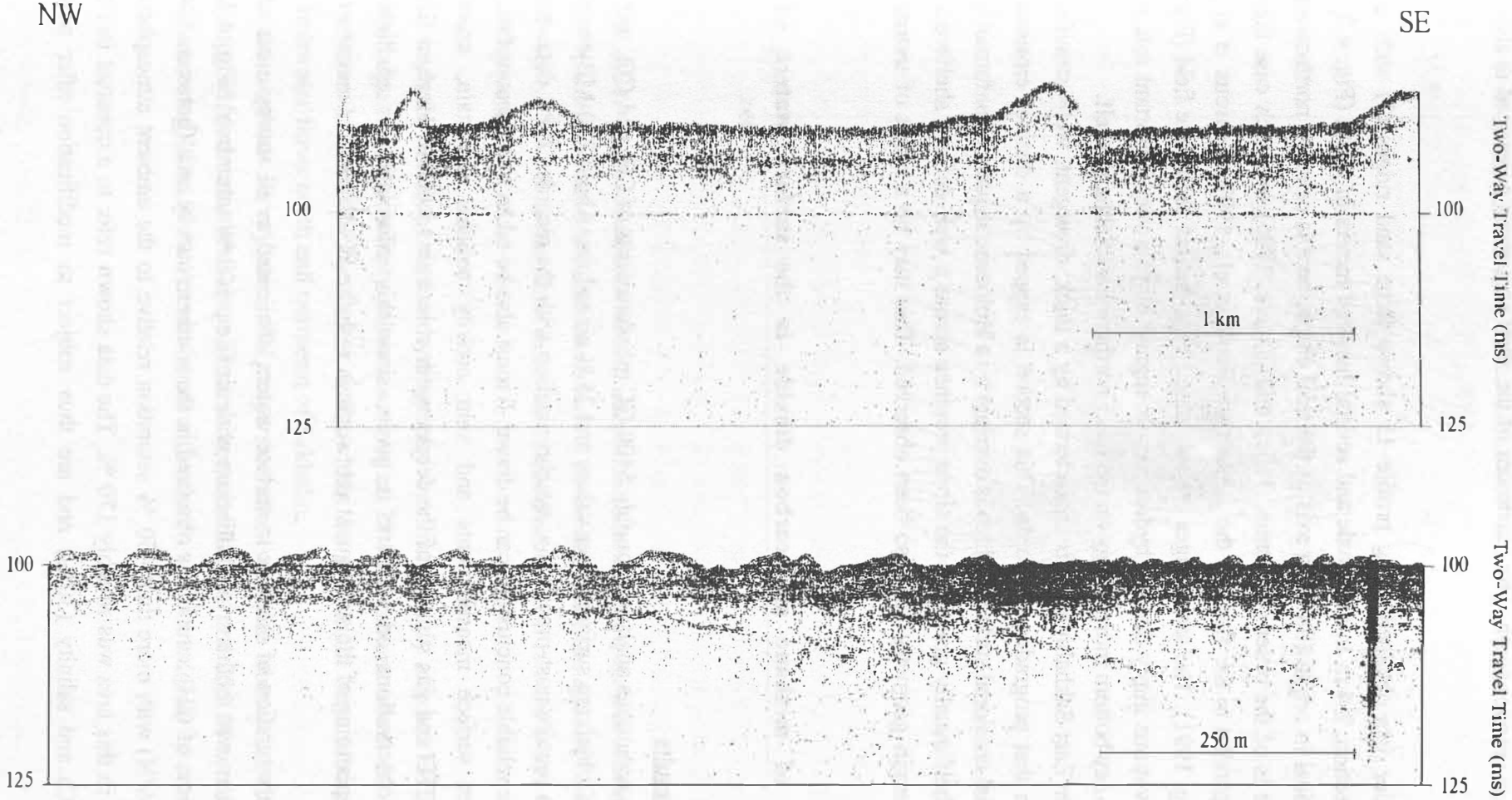

Fig. 4.9: *Part of echosounder profile 15 showing possible asymmetric sand ridges 2-4m in amplitude and several hundred meters in width. See Fig. 4.3 for profile location.*

Fig. 4.10: *Part of echosounder profile 15 showing a sandwave field. See Fig. 4.3 for profile location.*

sediment source as one moves south. The maximum of the shelf sequences penetrated is about 2 sec TWT.

3.5 kHz echosounder data obtained along profile 15 shows large sand ridges (?) with an asymmetric cross-section, 2-4 m in amplitude and several hundred meters in width (Fig. 4.9). They are possibly tidal in origin (the long axis of the tidal ellipse here is oriented north-south and the tidal current is of the order of 5 cm/s, Talley and Nagata, 1995) in which case they would be oriented parallel to the flow of the Amur (see Berné et al., 1997; Gensous et al., 1993; Nio and Yang, 1991). The sand ridges are succeeded by a distinct sandwave field (Fig. 4.10). These observations imply that the hydrodynamic regime plays a very important role in shaping the present-day bottom morphology on the inner northern East Sakhalin shelf.
In general, the inner East Sakhalin shelf is characterized by a thick, divergent, well- stratified sedimentary section that progrades seawards. This section is capped by a distinct erosional unconformity (glacial erosional surface) which is overlain by a Holocene sequence conformal to the seafloor. The shelf usually grades to the slope province across a well defined shelfbreak, although a ramp margin geometry has also been observed. This may be a result of tectonic influence.

4.3 Saturations of methane and carbon dioxide in the surface waters off Sakhalin

By S. Lammers

4.3.1 Preliminary results

During 15 days of continuous analyses, roughly 5400 GC measurements of CH_4 and CO_2 were performed, 50 % of which are surface water values and 25 % air values. About 250 MBytes of GC and sensor data require post-processing, synchronization with the recorded GPS data, and summarizing before reliable conclusions can be drawn. It must also be taken into account that a correlation between surface measurements and vent activity remains uncertain, unless information from CTD and gas surveys of the deeper water column is available. Here, a first overview on the observations on methane is given, since this information is of higher importance for the planning of the subsequent vent surveys with the *RV Akademik Lavrentyev.*

At first sight, supersaturation of methane in surface waters dominated in all survey areas off Sakhalin, only seldom was methane in equilibrium with air (i.e., 100 % saturation). Fig. 4.11 illustrates the maxima of CH_4 saturations observed in the southern survey area (between 144-145°W and 53-53.6°N) with more than 450 % saturation relative to the ambient atmosphere. The average value in this area was roughly 170 %. The data shown refer to a constant in-situ temperature (17° C) and salinity (30‰) and are thus subject to modification after post-processing.

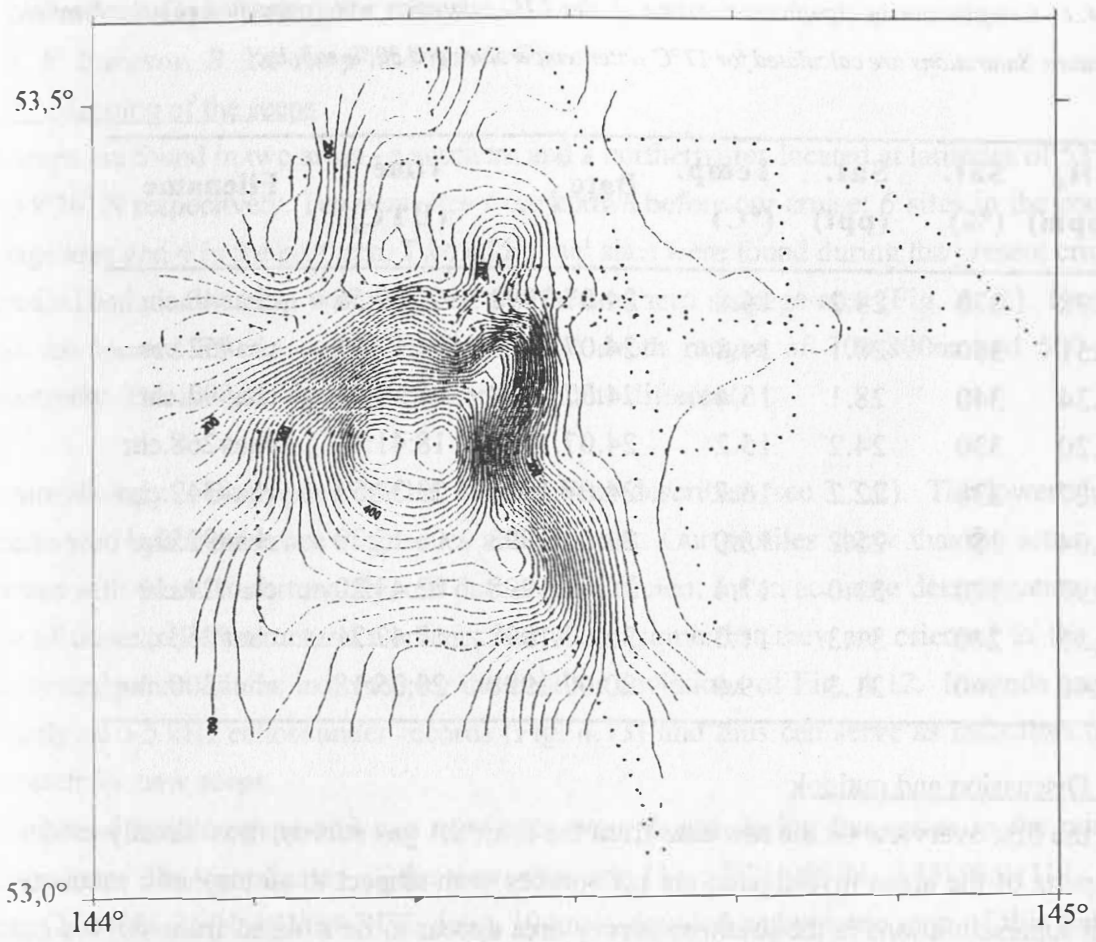

Fig. 4.11: *Methane saturation maxima observed in the southern seepage area (between 144-145°W and 53-53.6°N) with more than 450% saturation relative to the ambient atmosphere against an average value in this area of roughly 170%. These saturation values are calculated relative to a constant in-situ temperature (17°C) and salinity (30‰).*

Towards the north, the surface hydrography was increasingly affected by the Amur freshwater discharge, as local salinity minima as low as 23 ‰ (ambient: about 28 ‰) were recorded. Variation of salinities by almost 4 ‰ within 20 nm might be attributed to a fanning of freshwater flows north and northeast of Sakhalin.

In the northern survey area, CH_4 supersaturation was also abundant, although less intense compared to the southern area. Maxima between 370 % and 230 % were observed, ambient values being 120-150 %. A correlation with salinity was not evident.

Tab. 4.1: Compilation of significant maxima of the CH_4 saturation with associated values of salinity and temperature. Saturations are calculated for 17°C water temperature and 30 ‰ salinity.

CH_4 (ppm)	Sat. (%)	Sal. (ppt)	Temp. (°C)	Date	Time (UTC)	Filename
6.98	370	28.2	14.8	24.07.1998	03:19:56	cha#40.chr
6.51	350	28.1	14.8	24.07.1998	04:17:39	cha#52.chr
6.34	340	28.1	15.4	24.07.1998	06:57:43	cha#92.chr
6.20	330	24.2	15.2	24.07.1998	18:41:49	cha#268.chr
4.27	230	22.2	16.7	24.07.1998	23:37:52	cha#342.chr
7.04	380	25.2	15.0	26.07.1998	06:15:29	cha#92.chr
6.97	370	31.0	17.4	29.07.1998	02:43:20	cha#24.chr
4.55	240	31.3	11.3	30.07.1998	17:47:21	cha#258.chr
6.40	340	31.3	9.0	30.07.1998	20:35:18	cha#300.chr

4.3.2 Discussion and outlook

From the first overview on the raw data from the INESSA gas survey, it is already evident that most parts of the areas investigated are net sources with respect to atmospheric methane. The largest supersaturations in the southern survey area appear to be isolated from surface currents and may thus be the surficial image of an intensive venting located at about 700m water depth at the major fault zone of this area (cf. chapter 4.1, 4.4). The horizontal distance between the surface maximum and the presumed vent is roughly 5 nm in a NE-SW direction which parallels the prevailing water current. If this assumption is correct, it would be a remarkable height of the water column penetrated by a vent plume. Whether sources of methane other than venting (e.g., hydrographic features, *in situ* methanogenesis etc.) contribute to the overall supersaturation in this region needs to be clarified by the subsequent hydrographic surveys with the *RV Akademik Lavrentyev*.

As primarily intended, the data of the INESSA gas survey will permit an integration of the air-sea fluxes of methane and carbon dioxide over the study area. A major drawback in doing this is that data coverage is restricted to the region east of Sakhalin due to a severe delay of the cruise. The reliability of GPS recordings requires improvement on future expeditions. All in all, the combination of geophysical and surface gas surveys allows us to maximize both data resolution and ship time usage.

4.4 Areas of Gas Seepage

By B. V. Baranov, B. Ya. Karp and H. K. Wong

4.4.1 Mapping of the seeps

The seeps are found in two areas - a southern and a northern area located at latitudes of 53°25'N and 54°26' N respectively. Ten vent sites were known before our cruise: 6 sites in the southern seepage area and 4 in the northern. Two additional sites were found during the present cruise.

A detailed bathymetric map was prepared for the southern seepage area (Fig. 4.12). Here, the seeps are located in two zones, namely at the depth ranges of 700-800m and 500-600m respectively. The morphology of these zones is quite different.

The morphology of the upper slope has already been described (see 3.3.2). The lower slope is characterized by the existence of grooves and mounds. Our profiles show that the active seeps correlate with them. Unfortunately, our data are insufficient for an accurate determination of the strike of these (relief) structural elements; but we presume that they are oriented in the west-northwesterly direction as indicated by the contour deviations of Fig. 4.12. Mounds are seen distinctly on 3.5 kHz echosounder records (Fig. 4.13) and thus can serve as indicators during the search for new seeps.

Four sites of known seeps and two new sites were found during the cruise in the northern seepage area. The coordinates of the new sites are: (1) 54°21.959'N, 143°58.911'E, depth 390m; (2) 54°26.21'N, 143°54.24'E, depth 194m. A detailed bathymetric map of this field has been compiled earlier (Ginsburg et al., 1993), but regional profiles carried out during the present cruise yield new information on the morphology of this region. As the track spacing was rather large, we prepared the map manually (Fig. 4.14).

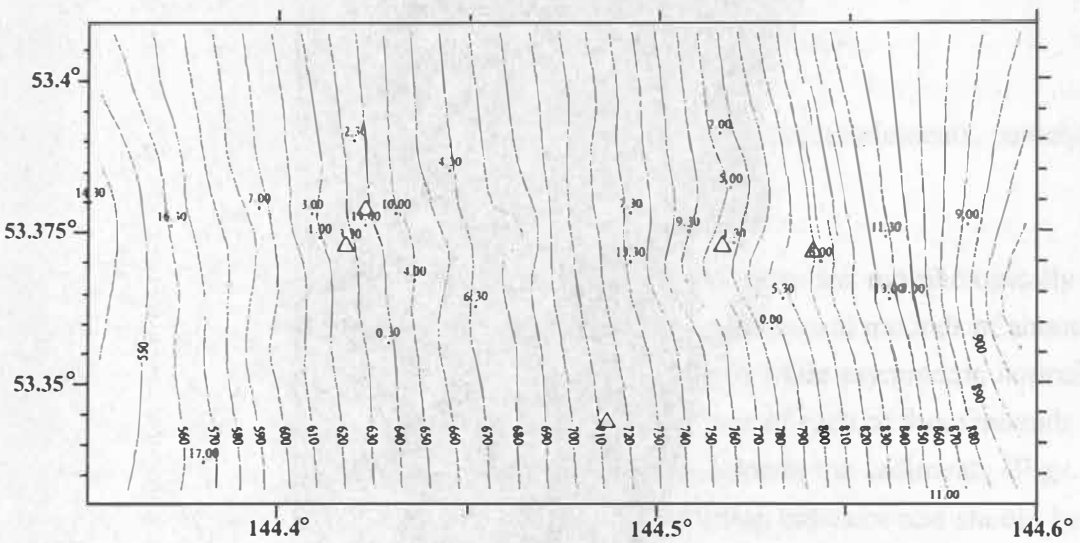

Fig. 4.12: Bathymetric map of the southern seepage area. Contour interval is 10m. Triangles indicate seep location. Dotted lines show tracks.

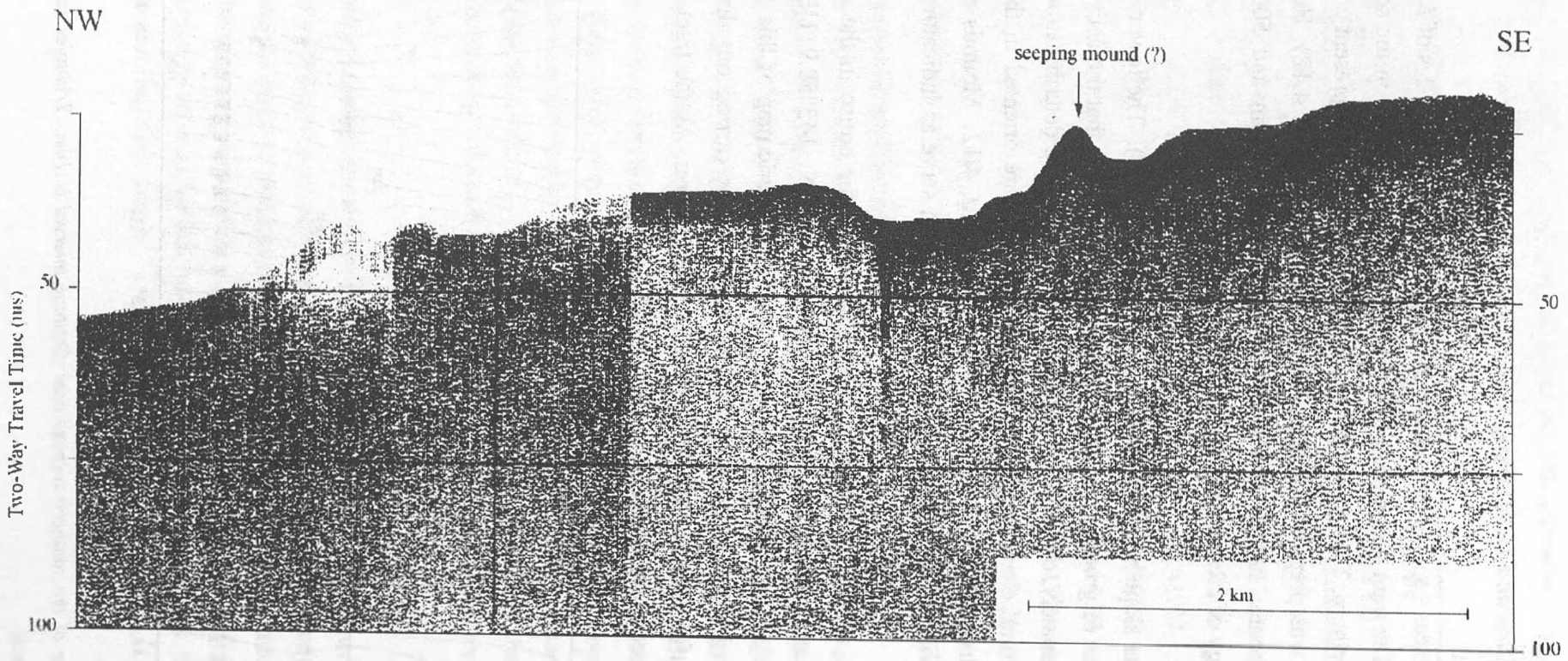

Fig. 4.13: Example of mound associated with a presumed seep. Part of profile 13, 3.5 kHz record.

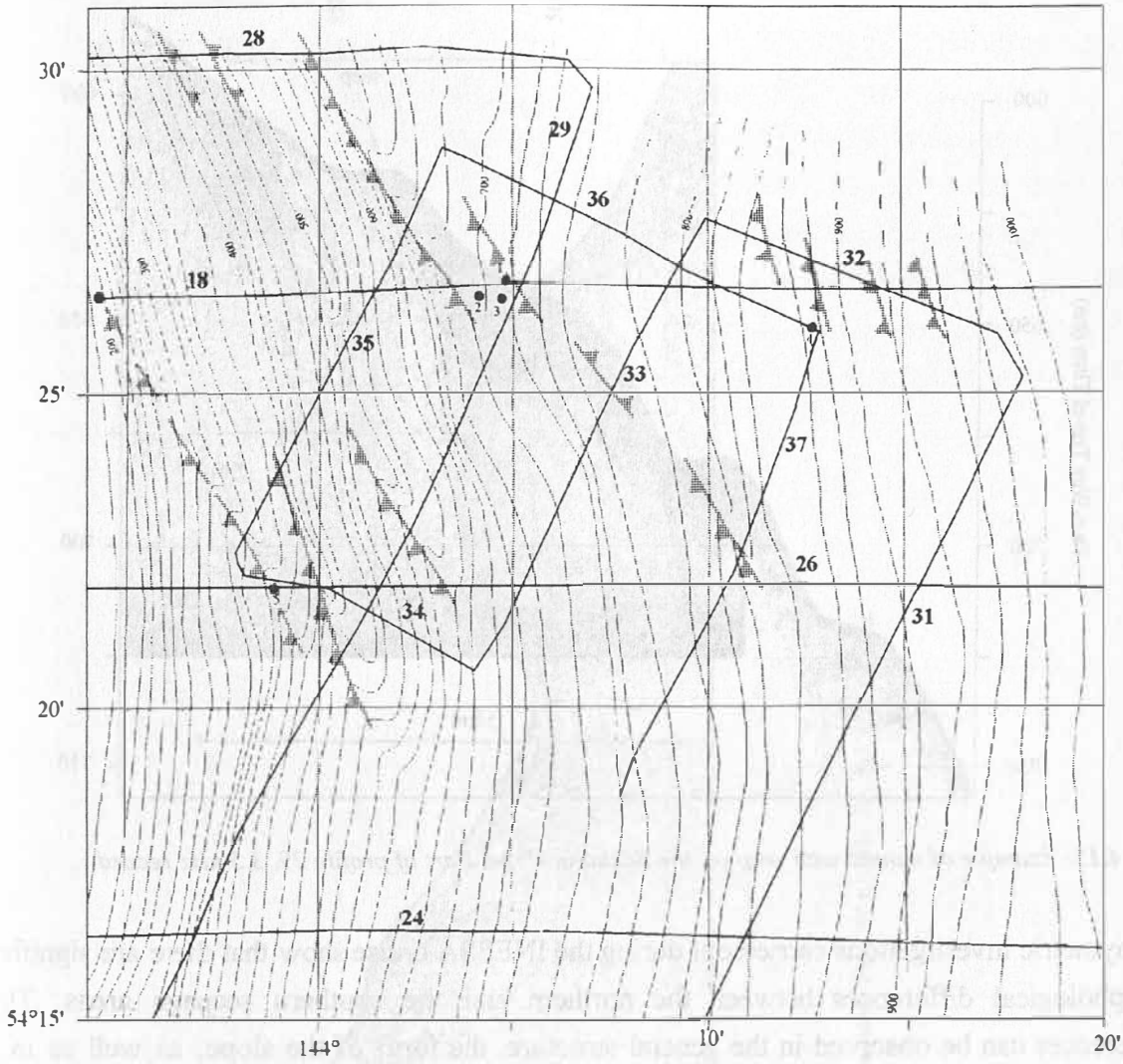

Fig. 4.14: Bathymetric map of the northern seepage area. Dots show seep locations.

It can be seen here that the seeps are well correlated with certain relief elements, namely with steps which are characteristic of the northern part of the slope.

3.5 kHz echosounder records demonstrate clearly that seep sites are morphologically quite different from the surrounding areas. Firstly, they represent symmetrical mounds of about 10 m in height. In addition, reverse fault scarps dominate in the north while asymmetric normal fault scarps exist in the south. Secondly, the upper sedimentary layers of each of these mounds curve up on echo-sounder records which point strongly to gas saturation in the sediments (Figs. 4.15 and 4.16). This fact should be regarded as a powerful prospecting indicator and should be used in the search for active vents.

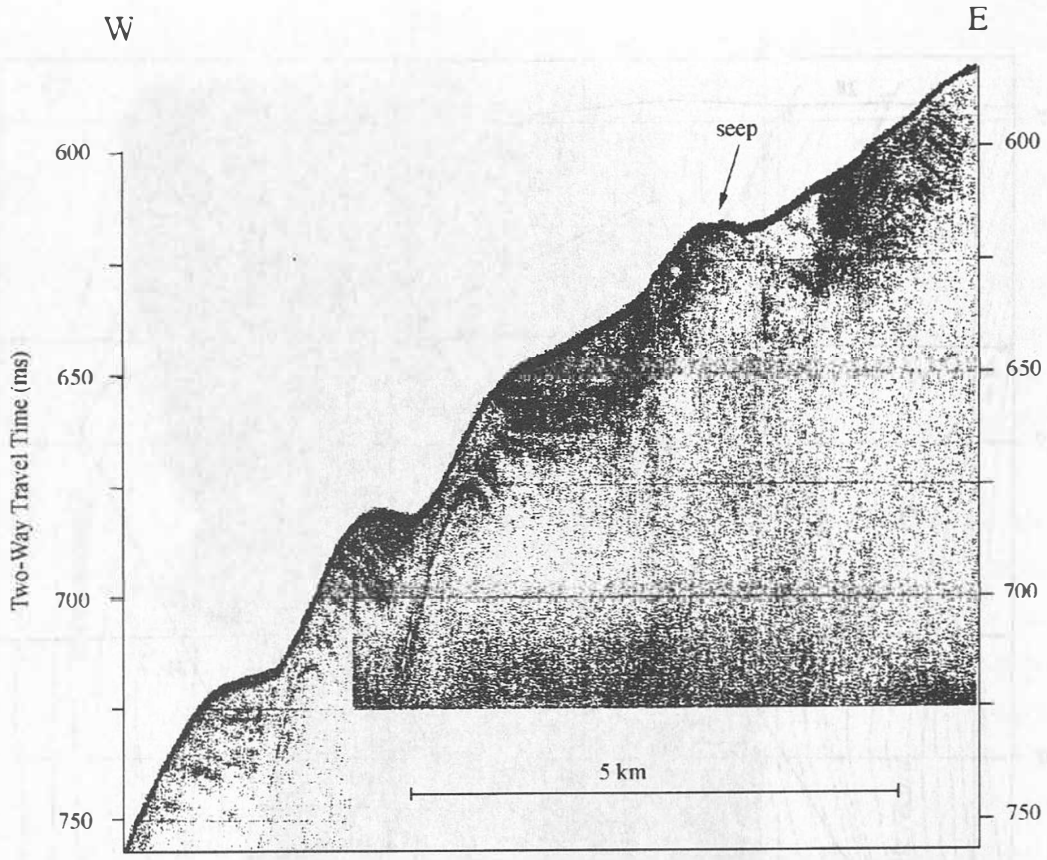

Fig. 4.15: Example of mound with seep on the Sakhalin slope. Part of profile 29, 3.5 kHz record.

Bathymetric investigations carried out during the INESSA cruise show that there are significant morphological differences between the northern and the southern seepage areas. These differences can be observed in the general structure, the form of the slope, as well as in the structure and character of its separate elements. Two explanations for these differences may be offered: the first is tectonic and the second in terms of the sedimentation regime. We will discuss the first possibility in chapter 5.2 while the second has been discussed in the section of this report on seismo-stratigraphy and sedimentation regime.

4.4.2 Botton simulating reflectors and the gas hydrate zone

High amplitude BSR's (bottom simulating reflector) which approximately follow the bottom relief are observed over extensive parts of the study area suggesting the widespread occurrence of gas hydrated-cemented sediments (Fig. 4.17; Hyndman and Davis, 1992; Hyndman and Spencer, 1992; Lee et al., 1994). Along profile 1 at water depths around 1,400m, the shallow BSR occurs at about 200 ms subbottom. It marks the upper boundary of the gas hydrate zone in which sediments cemented by gas hydrates are found. At depths shallower than this boundary, the hydrates are unstable and gas coexists in combination with pore water (Mienert and Posewang, 1997). A second, characteristically strong BSR cutting across the well-defined stratifications near the upper boundary of the middle sequence is found at greater depths (ca. 530 ms subbottom; see 3.1). It marks the lower boundary of the gas hydrate stability field. Its

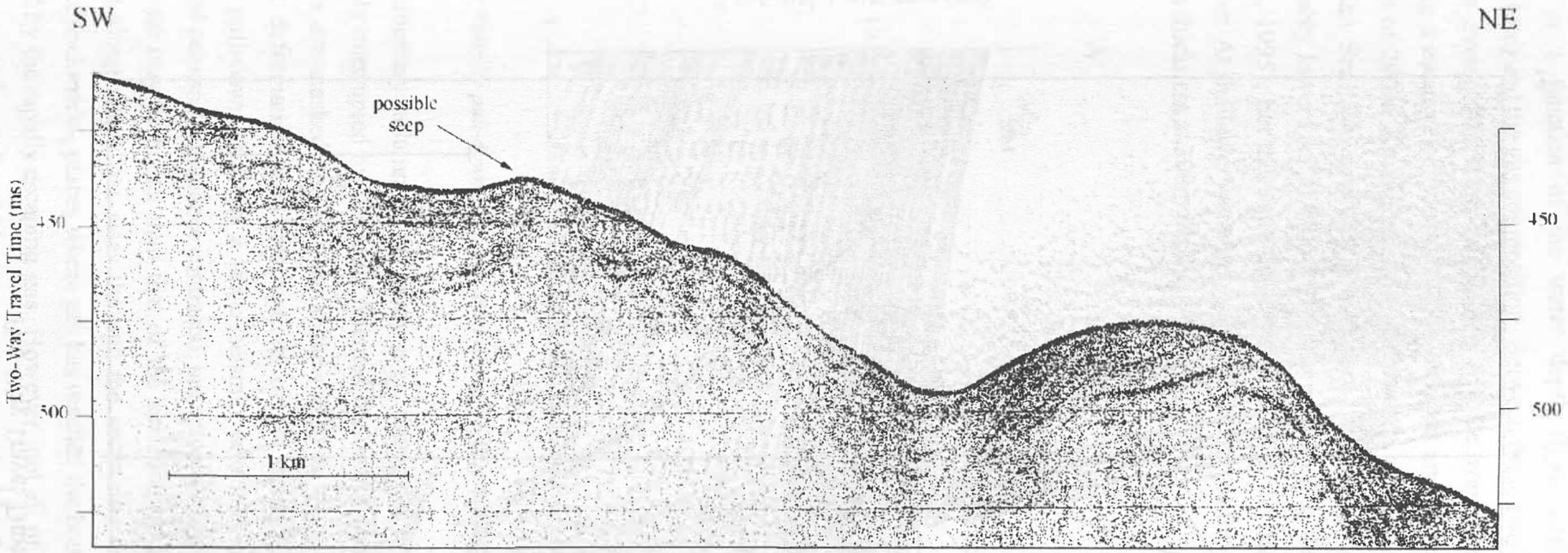

Fig. 4.16: Example of a possible seep with associated mound. Part of profile 26, 3.5 kHz record.

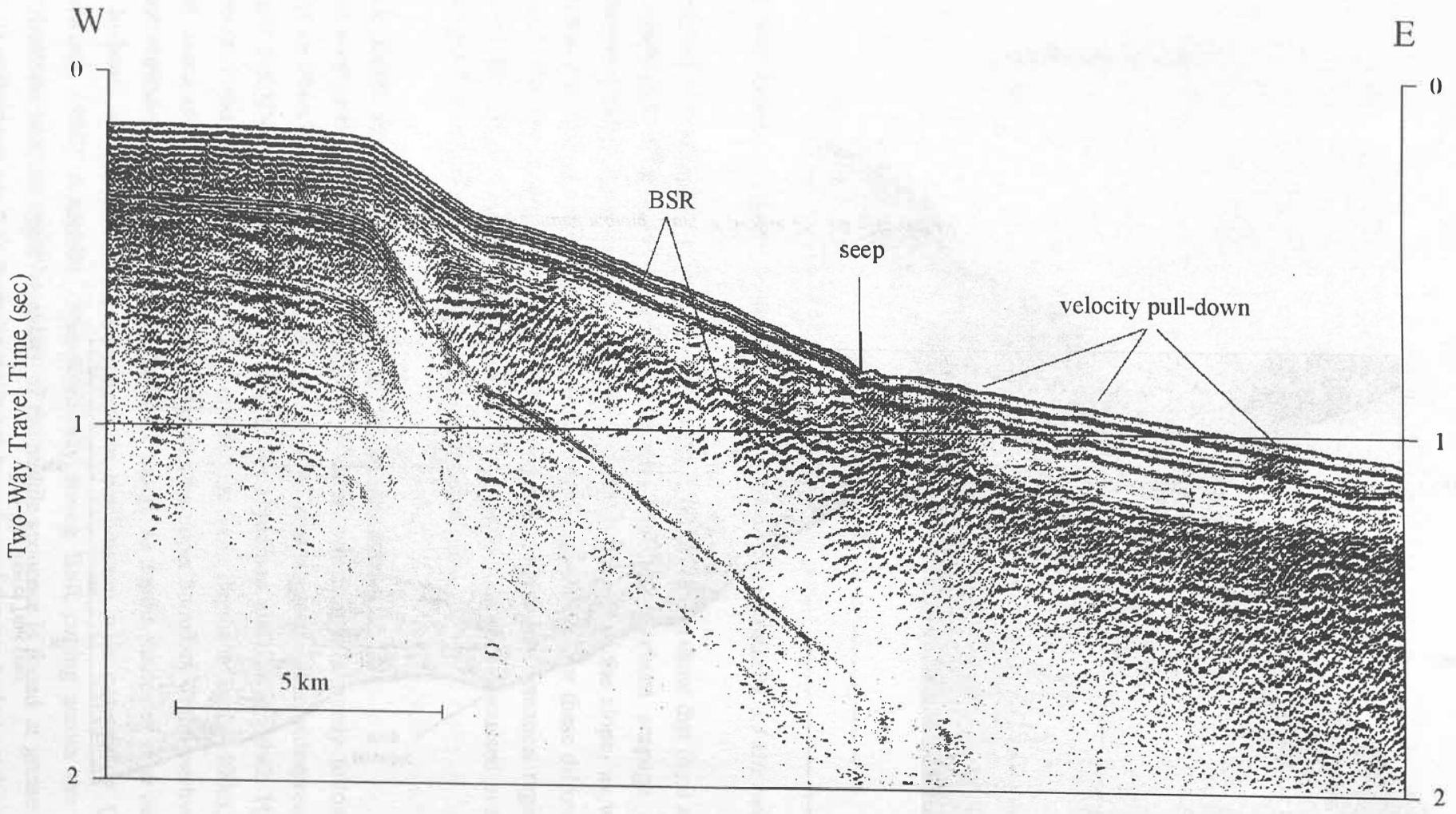

Fig. 4.17: Seismic profile showing a cross-section of seeps. Part of profile 18.

position is a function of the water depth (hydrostatic pressure), the thermal gradient (temperature) and the gas composition. Between these two BSR's, gas hydrate can coexist with gas. The average thickness of the gas hydrate zone along this profile is about 330 ms. Assuming a mean velocity of 1,780m/s (Mienert and Posewang, 1997), this corresponds to a thickness of 290m, a value which is comparable to that of 285m reported from the northern Norwegian Sea. We note that the surface geothermal gradient in the Norwegian Sea is considerably lower (5.5°C/100m) than that measured in the eastern Derugin Basin (8°C/100m; GERDA, 1995), but the water depth (1,000m) and the bottom temperature (at 65°N) are also both lower. At shallower water depths, the thickness of the gas hydrate stability zone is reduced (200m in thickness at 300m depth along profile 14).

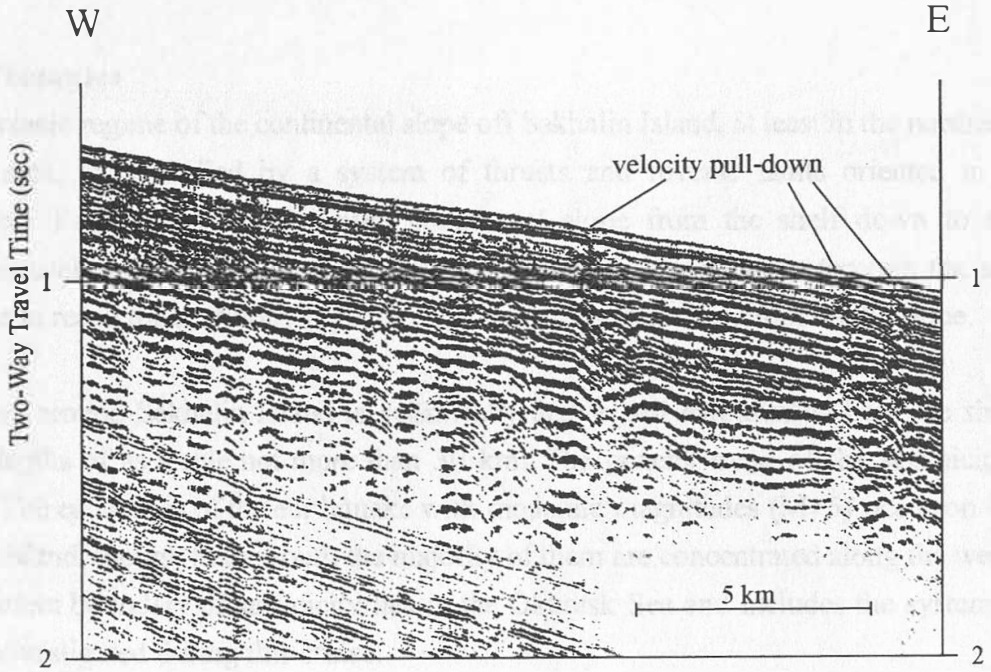

Fig. 4.18: Velocity pull-down structure. Part of profile 10, southern area.

The sedimentary column of the study area, especially that of the southern seepage area, is repeatedly interrupted by vertically oriented regions of acoustic turbidity in which some of the reflectors are masked and in general the reflection amplitudes are reduced. Typical are also apparent deformations and interruptions of the (mostly flat-lying) horizons. These include velocity pull-down (gas has a lower seismic velocity; Fig. 4.18) and increased amplitudes (enhanced acoustic impedance contrasts), but velocity pull-up is also common (mean velocity of gas hydrate may be higher than that of the surrounding sediment). These regions may mark channels along which gas rises through the sediments. Isolated troughs at the seafloor may represent pockmarks, places where gas has reached the bottom and sediments have been locally removed by the rapidly escaping gas. However, not all of these "pockmarks" are underlain by turbid zones and not all turbid zones are accompanied by "pockmarks".

Adjacent to the southern seepage area where the shelf is characterized by a ramp margin without a distinct shelfbreak, the lower BSR ascends from its normal depth towards the seafloor. The points of ascent lie within the water depth range of 450-550m. The 6 gas seeps with their accompanying plumes at the seafloor all occur near to but seawards of the points of ascent. Because these points can be correlated to thrusts, a causal relationship between thrust tectonics (and hence the partial destruction of the integrity of the gas hydrate zone with its consequent pressure release) and gas seepage is strongly suggested.

5. Conclusions

INESSA scientific party

KOMEX is a multidisciplinary project and encompasses a number of objectives related to a study of the Okhotsk Sea geosystem, in particular its structure and evolution. The INESSA expedition is directed at two of these objectives: (1) an investigation of the tectonic structure of the Okhotsk Sea, and (2) a study of the sedimentation history and paleo-environment. In addition, special attention is paid to the problem of a possible causal relationship between tectonic pattern and seep distribution. It is well known that such a relationship exists in subduction zones. Therefore, finding and formulating a similar relationship here and, based on this, making specific recommendations for the following geological and geochemical KOMEX cruise on the *RV Akademik Lavrentyev* was one of the important tasks of the present cruise.

5.1 Tectonics

The tectonic regime of the continental slope off Sakhalin Island, at least in the northern INESSA study area, is controlled by a system of thrusts and reverse faults oriented in a NW-SE direction. Faults exist on the entire continental slope from the shelf down to a depth of approximately 1,000m. These faults are active because they continue through the sedimentary column to reach the seafloor where they form scarps or step-like relief on the slope.

The area around Sakhalin Island is seismically active. All earthquakes here are shallow with focal depths of as a rule not more than 30 km. The general trend of the seismicity is north-south. The epicentres of the earthquake with moderate magnitudes (M>5) occur on both flanks of this island, though to the south the majority of them are concentrated along the western coast. The eastern boundary of seismicity lies in the Okhotsk Sea and includes the system of reverse faults investigated during this cruise.

It is reasonable to assume that the tectonic pattern offshore Sakhalin corresponds to that of Sakhalin Island. As is already known, the main structure of the Sakhalin Island is the Central Sakhalin Fault (Fig. 5.1). It extends for a distance of 600 km and disappears in the north under Quaternary sediments and in the south in the La Peruse Strait between Sakhalin and Hokkaido. The Central Sakhalin Fault strikes almost north-south, being slightly distorted near 142° and 143°E. It consists of a series of almost linear segments. The longest among them are oriented in the northwesterly direction (340-0°) and are displaced relative to each other by shorter segments represented by right-lateral strike-slips striking from N10°E to N45°E. The ratio of the long to the short segments determines fault stretching in general. These faults extend from the southern part of the island in a north-northeastern direction to the northern edge of Terpeniya Bay and consist of many right-lateral strike-slips in between. Farther to the north its strike changes to north-northwest because there are not

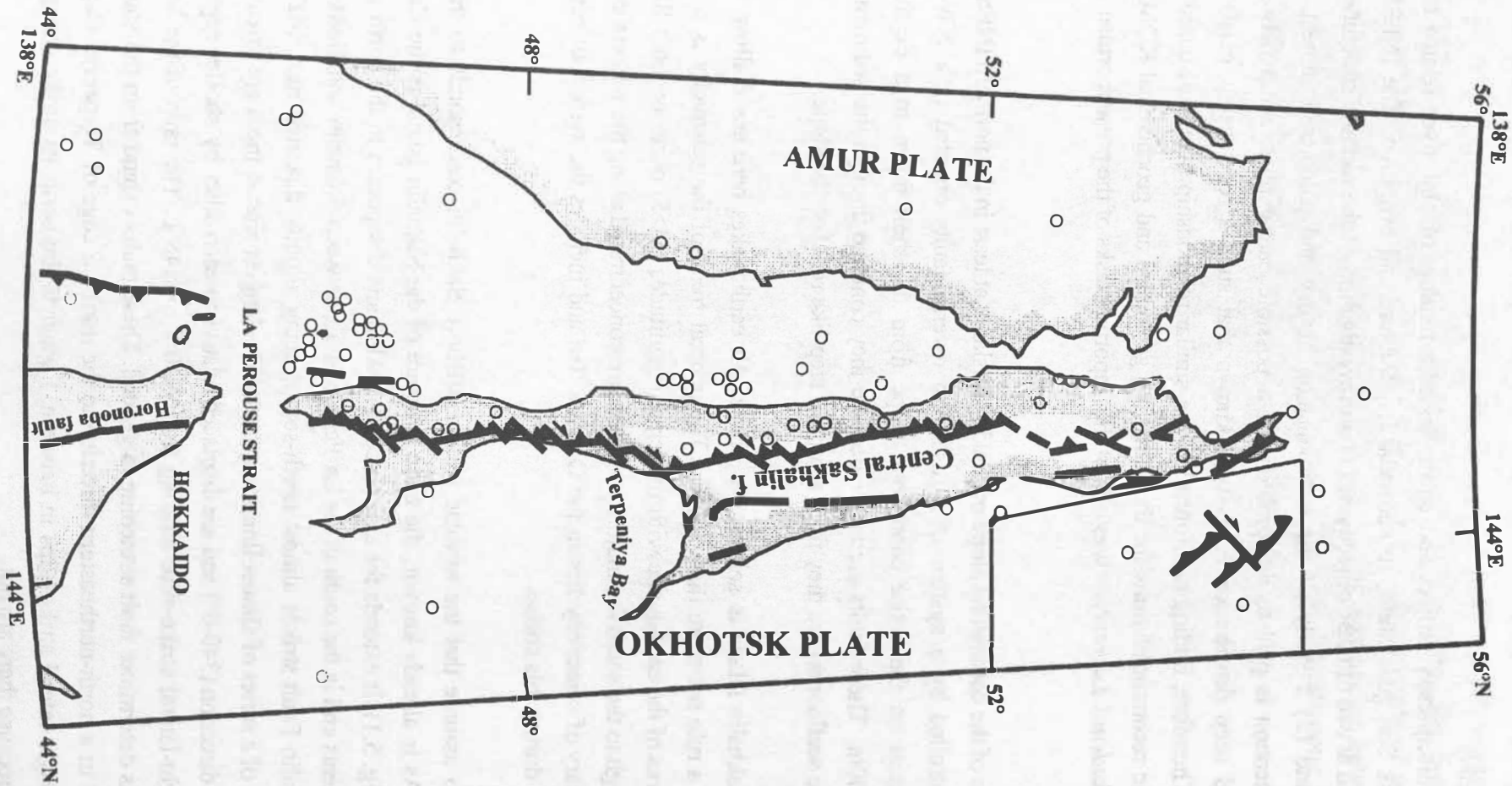

Fig. 5.1: Tectonic structure of Sakhalin Island and the INESSA area (dashed line). Lines with teeth mark reverse faults, lines with arrow indicate strike-slips. Dotted line shows eastern boundary of the Sakhalin seismic belt. Thin lines give contours of gravity anomalies.

many strike-slips in this segment. Detailed structural investigations carried out on the short as well as on the long fault segments demonstrate that the former are almost pure dextral strike-slips and the latter are thrusts with a strike-slip component (Fournier et al., 1994). This structural pattern corresponds to the orientation of faults mapped during the INESSA cruise.

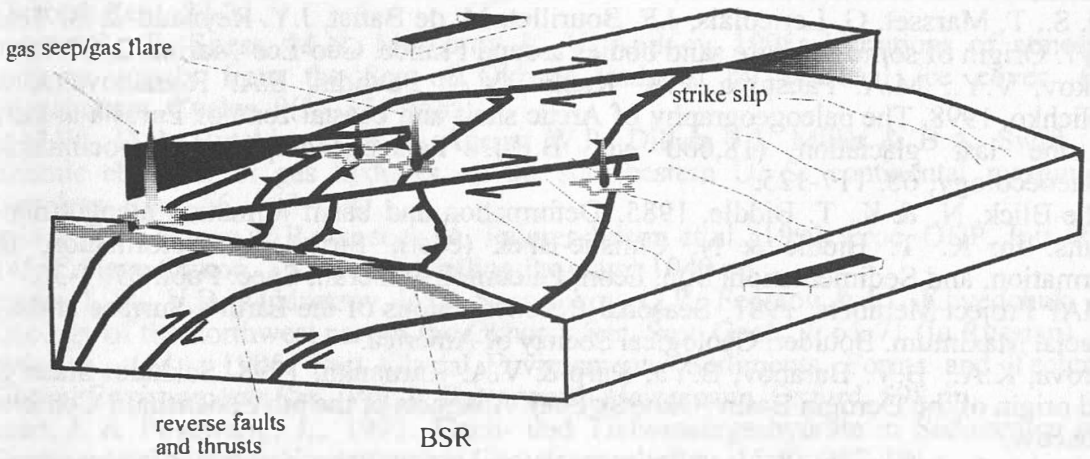

Fig. 5.2: Cartoon of the offshore structure and seep locations in the Sakhalin Shear Zone.

5.2 Seep distribution

The character of seep distribution on the eastern Sakhalin margin suggests that gas seeps correlate with certain tectonic zones and are directly controlled by the tectonic regime. It is obvious that for the northern area, all known seeps are located near reverse faults generated under conditions of NE-SW compression. The structural pattern existing here is similar to the tectonic regime in subduction zones, especially in those with a thick sedimentary cover (Oregon type) where gas conduits are represented by reverse faults and thrusts (Fig. 5.2).

6. REFERENCES

Alperovich, I.M. & G.A. Chernyavsky, 1973. Report of the „Hecauteus" Expedition-1 in the Okhotsk Sea, 1966. Oceanogr. Mag., 19, 57-59.

Anderson, J.B. & B.F. Molnia, 1989. Glacial-Marine Sedimentation. Short Course in Geology, 9, Amer. Geophys. Un., Washington, D.C., 127 pp.

Baranov, B.V., K.A. Dozorova & A.S. Svarichevsky, 1995. Cenozoic kinematics of the Okhotsk plate: opening of the back-arc basin and Okhotsk rift system. Abstracts of the International Lithosphere Program Workshop, Miyagi, Japan.

Baranov, B.V., B.Ya. Karp, T. Dickmann, K.A. Dozorova & V.N. Karnaukh, in press. Tectonics of the central Ionian Rift, eastern Derugin Basin (Okhotsk Sea). Tectonics.

Berné, S., T. Marsset, G. Lericolais, J.F. Bourillet, M. de Batist, J.Y. Reynaud & B. Tessier, 1997. Origin of some offshore sand bodies around France. Geo-Eco-Marina, 2, 57-76.

Biryukov, V.Y., M.A. Faustova, P.A. Kaplin, Y.A. Pavlidis, E.A. Romanova & A.A. Velichko, 1998. The paleogeography of Arctic shelf and coastal zone of Eurasia at the time of the last glaciation (18,000 yr. B.P.). Palaeogeography, Palaeoclimatology, Palaeoecology, 68, 117-125.

Christie-Blick, N. & K. T. Biddle, 1985. Deformation and basin formation along strike-slip faults. In: K. T. Biddle & N. Christie-Blick (eds.), Strike-Slip Deformation, Basin Formation, and Sedimentation. Soc. Econ. Paleontol. Mineral., Spec. Publ. 37, 1-34.

CLIMAP Project Members, 1981. Seasonal Reconstructions of the Earth's Surface at the Last Glacial Maximum. Boulder, Geological Society of America.

Dozorova, K.A., B.V. Baranov, B.Ya. Karp & V.A. Karnaukh, 1998. Sakhalin Shear Zone and origin of the Derugin Basin (Okhotsk Sea). Abstracts of the 6th Zonenshain Conference, Moscow.

Fournier M., L. Jolivet, Ph. Huchon, K.F. Sergeyev & L.S. Oscorbin, 1994. Neogene strike-slip faulting in Sakhalin and Japan Sea opening. Journ. Geoph. Res., 99, 2701-2725.

Gensous, B., D. Williamson & M. Tesson, 1993. Late-Quaternary transgressive and highstand deposits of a deltaic shelf (Rhône delta, France). Spec. Publs. Int. Ass. Sediment., 18, 197-211.

GERDA, 1995. Report of R/V Professor Gagarinskiy Cruise 16 „GERDA": Geophysical Research in the Derugin Basin Area (the Okhotsk Sea), 36 pp.

Ginsburg, G.D., V.A. Soloviev, R.E. Cranston, T.D. Lorenson & K.A. Kvenvolden, 1993. Gas hydrates from continental slope, offshore Sakhalin Island, Okhotsk Sea. Geo-Marine Letters, 13, 41-48.

Gnibidenko, H.S. & I.I. Khvedchuk, 1982. The tectonics of the Okhotsk Sea. Mar. Geol. 50, 155-198.

Gnibidenko, H.S. & A.S. Svarichevsky, 1984. Tectonics of the Okhotsk deep-sea basin. In: R.L. Carlson & K. Kobayashi (eds.), Geodynamics of the Backarc Regions, Tectonophys., 102, 225-244.

Gorbarenko, S.A., N.N. Kovalyukh, L.Yu. Odinokova, V.F. Rybakov, T.N. Tokarchuk & V.V. Shapovalov, 1990. Upper Quaternary sediments of the Sea of Okhotsk and the reconstruction of paleoceanologic conditions. Geol. of Pac. Ocean., 6(2), 309-330.

Grosswald, M.G., in press. Late Weichselian ice sheets in Arctic and Pacific Siberia. Quaternary International.

Grosswald, M.G. & T.J. Hughes, 1998. Evidence for Quaternary glaciation of the Sea of Okhotsk. In: S. Horie (ed.), International Project on Paleolimnology and Late Cenozoic Climate (IPPCCE) Newsletter No. 11, 3-25.

Harding, T.P., R.F. Gregory & L.H. Stephens, 1983. Convergent wrench fault and positive flower structure, Ardmore Basin, Oklahoma. In: A.W. Bally (ed.), Seismic Expression of Structural Styles. Amer. Assoc. Petr. Geol., Studies Geol., 15(3), 4.2-13-4.2-17.

Hughes, T.J., 1995. A search for marine ice sheets in Pleistocene Beringia. In: Simakov, K.V. (ed.), Proceedings of the International Conf. on Arctic Margins, Magadan, Russia, Sept. 1994, 81-94.

Hyndman, R.D. & E.E. Davis, 1992. A mechanism for the formation of methane hydrate and seafloor bottom-simulating reflectors by rapid fluid expulsion. Journ. Geophys. Res., 97(B5), 7025-7041.

Hyndman, R.D. & G.D. Spencer, 1992. A seismic study of methane hydrate marine bttom simulating reflectors. Journ. Geophys. Res., 97(B5), 6683-6698.

Jolivet L., P. Huchon, J.P. Brun, N. Chamot-Rooke, X. Le Pichon & J.C. Thomas, 1991. Arc deformation and marginal basin opening: Japan Sea as a case study. Journ. Geophys. Res., 96, 4367-4384.

Kaiko-Tokai project, 1998. Tectonics of subduction in the Nankai Trough. International Symposium on Japan - France Kaiko - Tokai Project, Abtract Vol., 82 pp.

Karp, B., V. Karnaukh & T. Dickmann, 1995. Seismics. In: Report of R/V Professor Gagarinskiy Cruise 16 „GERDA": Geophysical Research in the Derugin Basin Area (the Okhotsk Sea), 24-31.

Lammers, S., E. Suess, M.N. Mansurov &, V. Anikiev, 1995. Variations of atmospheric methane supply from the Sea of Okhotsk induced by seasonal ice cover. Global Biogeochem. Cycles, 9(3), 351-358.

Lee, M.W., D.R. Hutchinson, W.F. Agena, W.P. Dillon, J.J. Miller & B.A. Swift, 1994. Seismic character of gas hydrates on the southeastern U. S. continental margin. Mar. Geophys. Res., 16, 163-184.

Rea, D.K., I.A. Basov, T.R. Janecek, A. Palmer-Julson et al., 1993. Proc. ODP, Init. Repts., 145, College Station, TX (Ocean Drilling Program) 1040 pp.

Margulis, L.S., V.B. Mudretzov, B.G. Sapojnikov, G.P. Fedotov & I.I. Khvedchuk, 1979. Geology of the northwest part of the Okhotsk Sea. Sov. Geol., 7, 61-71 (in Russian).

Menzies, J., (ed.), 1995. Past Glacial Environments: Sediments, Forms and Techniques. Glacial Environments Ser., Vol. 2, Butterworth-Heinemann, Oxford, 598 pp.

Mienert, J. & Posewang, J., 1997. Flach- und Tiefwassergashydrate in Sedimenten polarer Kontinentalränder des Nordatlantiks. Geowissenschaften, 15(9), 287-291.

Milliman, J.D. & R.H. Meade, 1983. World-wide delivery of river sediments to the oceans. J. Geol., 91(1), 1-21.

Nio, S.D. & C.S. Yang, 1991. Sea-level fluctuations and the geometric variability of tide-dominated sandbodies. In: K.T. Biddle & W. Schlager (eds.), The Record of Sea-Level Fluctuations. Sediment. Geol., 70, 161-193.

Nürnberg, D., Baranov, B.V., Karp, B.Ya. (eds.), 1997. RV Akademik Lavrentyev cruise 27 - cruise report Gregory, Geomar Report, 60, 69 pp.

Rea, D.K., I.A. Basov & Janecek, T.R., 1993. Cenozoic paleoceanography of the North Pacific Ocean; Results of ODP Leg 145, the North Pacific transects. Eos Transactions, 74, 173.

Rehder, G., 1996. Quellen und Senken marinen Methans zwischen Schelf und offenem Ozean. Diss. Univ. Kiel.

Rozhdestvenskiy, S.S., 1982. The role of wrench faults in the structure of Sakhalin. Geotectonics, 16, 323-332 (in Russian).

Rozhdestvenskiy, S.S., 1986. Evolution of the Sakhalin fold system. Tectonophysics, 127, 331-339.

Savostin, L.A., L.P. Zonenshain & B.V. Baranov, 1983. Geology and plate tectonics of the Sea of Okhotsk, In: Hilde T.W.C. and Uyeda S. (eds.), Geodynamics of the Western Pacific-Indonesian Region. Geodynamic Series AGU, 11, 189-222.

Syvitski, J., A.K. Cooper & M.S. Stoker, (eds.), 1997. COLDSEIS (Seismic Facies of Glacigenic Deposits). Spec. Issue, Mar. Geol., 143, 1-262.

Talley, L.D. & Y. Nagata (eds.), 1995. The Okhotsk Sea and Oyashio Region. North Pacific Marine Science Organisation (Report of Working Group 1). Pices Scientific Rept. No. 2, 227 pp.

Velichko, A.A., (ed.), 1993. Climate and Landscape Evolution in Northern Eurasia, the Late Pleistocene and Holocene. Moskva, „Nauka" (in Russian).

Vogt, C., J. Grützner, S. Gorbarenko, A. Astakhov & D. Nürnberg, 1997. Sedimentation at the northeastern slope of Sakhalin. In: Cruise Report of the R/V Akademik M.A. Lavrentyev Cruise 27 „Gregory": German-Russian Expedition for Geological/ Geophysical Okhotsk Sea Research. GEOMAR Report, 60, 41-43.

Zanyukov V.N., 1972. The central Sakhalin fault and its role in the tectonic evolution of the island. Papers of the Acad. Sci. USSR (in Russian).
Zhuravlev, A.V., 1984. Comparison between the Derugin and Tinro basins of the Okhotsk Sea. Geology of the Pacific, 4, 21-27 (in Russian).

Appendices

Appendix 1

List of profiles KOMEX 98, cruise 22 of the RV Professor Gagarinsky, Sea of Okhotsk, July 98

Profile No.	Start				End				Course	Duration	Distance	
	Date (d.mm.yy)	Time (hh:min)	Latitude (N)	Longitude (E)	Date (d.mm.yy)	Time (hh:min)	Latitude (N)	Longitude (E)	(°)	(hh:min)	nm	km
1	20.07.98	12:30	51°12.86	146°42.16	21.07.98	00:20	52°09.24	147°03.87	13	11:50	57.6	106.7
2	21.07.98	01:05	52°08.50	147°05.27	21.07.98	04:25	51°52.88	147°12.41	162	03:20	16.6	30.7
3	21.07.98	04:39	51°52.59	147°10.97	22.07.98	07:16	53°22.46	144°56.18	316	26:37	121.0	224.0
4	22.07.98	10:33	53°21.15	144°52.01	22.07.98	15:44	53°23.56	144°10.42	274	05:11	25.2	46.7
5	22.07.98	15:52	53°23.59	144°09.76	22.07.98	16:24	53°26.57	144°09.77	360	00:32	3.0	5.6
6	22.07.98	16:34	53°26.99	144°10.52	22.07.98	20:31	53°28.17	144°42.08	86	03:57	18.5	34.2
7	22.07.98	20:50	53°27.07	144°42.64	22.07.98	22:56	53°17.44	144°43.66	174	02:06	10	18.5
8	22.07.98	23:15	53°16.91	144°41.88	23.07.98	03:37	53°17.63	144°10.36	270	04:22	19.2	35.6
9	23.07.98	03:43	53°17.36	144°10.04	23.07.98	05:39	53°09.96	144°10.44	178	01:56	7.0	12.9
10	23.07.98	05:47	53°09.78	144°11.35	23.07.98	09:04	53°09.80	144°38.00	90	03:17	16.2	30.0
11	23.07.98	09:15	53°10.46	144°38.62	23.07.98	13:24	53°31.19	144°28.90	345	04:11	21.8	40.0
12	23.07.98	13:37	53°31.72	144°27.65	23 07.98	14:23	53°31.87	144°21.51	270	00:46	3.6	6.6
13	23.07.98	14:31	53°31.39	144°20.98	23.07.98	20:22	53°06.90	144°31.75	164	05:51	24.9	46.0
14	24.07.98	08:54	53°22.56	144°35.58	24.07.98	16:13	53°19.50	143°34.34	266	07.19	37.1	68.7
15	24.07.98	16:18	53°19.79	143°33.86	24.07.98	22:05	53°54.12	143°20.27	348	05:47	35.0	64.8
16	24.07.98	22:18	53°54.82	143°21.95	25.07.98	08:25	53°53.30	144°50.06	92	10:07	51.9	96.1
17	25.07.98	08:31	53°53.66	144°50.39	25.07.98	15:16	54°25.95	144°33.81	341	06:45	33.3	61.7
18	25.07.98	15:22	54°26.31	144°33.11	26.07.98	01:55	54°26.21	143°05.63	272	10:33	50.6	93.7
19	26.07.98	02:02	54°25.81	143°05.31	26.07.98	05:52	54°05.96	143°12.18	167	03:50	20.4	37.8
20	26.07.98	05:55	54°05.66	143°12.46	26.07.98	15:35	54°06.89	144°20.36	92	09:40	39.9	73.9
21	26.07.98	15:41	54°07.17	144°20.85	26.07.98	16:29	54°10.49	144°20.22	355	00:48	3.1	5.7
22	26.07.98	16:36	54°10.49	144°19.45	26.07..98	19:50	54°11.57	143°50.00	272	03:14	17.1	31.7
23	26.07.98	19:55	54°11.88	143°49.73	26.07.98	20:45	54°16.32	143°50.38	5	00:50	4.0	7.4
24	26.07.98	20:49	54°16.35	143°50.83	27.07.98	00:37	54°16.14	144°21.42	92	03:48	17.5	32.4
25	27.07.98	00:42	54°16.56	144°21.56	27.07.98	01:46	54°21.58	144°21.71	360	01:04	5.0	9.3
26	27.07.98	01:50	54°22.01	144°21.29	27.07.98	06:00	54°21.87	143°50.93	270	04:10	17.5	32.4
27	27.07.98	06:05	54°22.10	143°49.61	27.07.98	07:51	54°29.99	143°48.68	358	01:46	8.0	14.8
28	27.07.98	07:56	54°30.60	143°49.12	27.07.98	10:06	54°30.44	144°06.24	90	02:10	9.9	18.3

Profile No.	Start				End				Course	Duration	Distance	
	Date (d.mm.yy)	Time (hh:min)	Latitude (N)	Longitude (E)	Date (d.mm.yy)	Time (hh:min)	Latitude (N)	Longitude (E)	(°)	(hh:min)	nm	km
29	27.07.98	10:17	54°29.82	144°07.15	27.07.98	16:58	54°03.39	143°49.59	202	06:41	28.8	53.3
30	27.07.98	17:06	54°03.06	143°50.06	27.07.98	18:50	54°00.33	144°02.44	112	01:44	7.7	14.3
31	27.07.98	18:56	54°00.58	144°03.13	28.07.98	00:16	54°15.28	144°18.05	20	05:20	16.5	30.6
32	28.07.98	00:27	54°25.93	144°17.48	28.07.98	01:25	54°27.72	144°10.30	291	00:58	4.5	8.3
33	28.07.98	01:30	54°27.57	144°09.76	28.07.98	03:05	54°20.79	144°04.37	201	01:35	7.8	14.4
34	28.07.98	03:11	54°20.76	144°03.76	28.07.98	04:02	54°22.26	143°57.83	300	00:51	3.6	6.7
35*	28.07.98	04:06	54°22.53	143°57.95	28.07.98	05:23	54°28.97	144°03.18	28	01:17	6.7	12.4
36*	28.07.98	05:29	54°28.91	144°03.78	28.07.98	06:39	54°26.10	144°12.65	115	01:10	6.0	11.1
37*	28.07.98	06:43	54°25.75	144°12.79	28.07.98	08:20	54°18.46	144°07.36	202	01:37	8.7	16.1
38*	28.07.98	08:20	54°18.46	144°07.36	28.07.98	14:51	53°49.32	144°09.00	180	06:31	29.0	53.7
39	28.07.98	14:57	53°49.18	144°09.49	29.07.98	07:45	53°49.17	146°02.92	90	16:48	67.3	124.6
40	29.07.98	07:53	53°48.68	146°03.43	30.07.98	00:24	52°41.05	145°23.02	200	16:31	72.1	133.5
41	30.07.98	00:27	52°41.01	145°22.98	30.07.98	09:16	52°12.33	144°29.94	228	08:49	43.4	80.4
42	31.07.98	08:17	50°05.09	147°30.59	31.07.98	21:00	49°09.01	146°34.88	213	12:43	66.7	123.5
									Total	**212:51**	**1041.2**	**1969.1**
									Total: airgun profiles	**202:16**	**990.8**	**1877.8**

* no airgun profiles

Appendix 2

List of participants

1. Dr. Boris Karp	Co-Chief Scientist, seismics (POI, FED RAS)
2. Prof. How Kin Wong	Co-Chief Scientist, mar. geophysics (IfBM, UniHH)
3. Dr. Nicole Biebow	Marine geology (GEOMAR)
4. Dr. Boris Baranov	Tectonics (IO, RAS)
5. Mrs. Karina Dozorova	Tectonics (IO, RAS)
6. Mr. Martin Jovanovic	Seismics (IfBM, UniHH)
7. Dr. Viktor Karnaukh	Seismics (POI, FED RAS)
8. Mrs. Tatyana Kolpashchikova	Gravity (POI, FED RAS)
9. Dr. Sergei Nikolaev	Gravity (POI, FED RAS)
10. Dr. Stefan Lammers	Geochemistry (GEOMAR)
11. Dr. Thomas L¸dmann	Seismics (IfBM, UniHH)
12. Mr. Matthias Lurati	Seismics (IfBM, UniHHU)
13. Ms. Alke-Marit Paulsen	Seismics (IfBM, UniHH)
14. Mr. Anatoly Sudakov	Seismics (POI, FED RAS)
15. Mr. Nikolay Tsovbun	Magnetics (POI, FED RAS)

GEOMAR:	Research Center for Marine Geosciences, Christian-Albrechts-University, Kiel
IfBM, UniHH:	Institute of Biogeochemistry and Marine Chemistry, Hamburg University, Hamburg
IO RAS:	P. P. Shirshov Institute of Oceanology, Russian Academy of Sciences, Moscow
POI FED RAS:	Pacific Oceanology Institute, Far Eastern Division of the Russian Academy of Sciences, Vladivostok